




Recent developments in transition metal-based nanomaterials for supercapacitor applications

Rahul Singhal^{1,a)} , Manika Chaudhary², Shrestha Tyagi², Deepanshi Tyagi², Vanshika Bhardwaj², Beer Pal Singh^{2,a)}

¹Department of Physics and Engineering Physics, Central Connecticut State University, New Britain, CT 06050, USA

²Department of Physics, Chaudhary Charan Singh University, Meerut 250004, India

^{a)}Address all correspondence to these authors. e-mails: singhal@ccsu.edu; drbeerpal@gmail.com

Received: 18 February 2022; accepted: 9 May 2022; published online: 2 June 2022

In the recent years the demand of high energy density, high power density energy storage device with long cycle stability increased because of their vast applications from portable electronics devices to power tolls and hybrid electric vehicles. Also, the developments in renewable energy sources also created immediate demand for high energy density energy storage devices. Supercapacitors are found to be suitable to fulfill the current demand of energy storage devices. Transition metal nanomaterials are considered to store high charge because of their large surface area and variable oxidation states. In the present review, we discussed the recent advances in the area of supercapacitors using transition metal oxides, nitride, sulfides, diselenides, phosphides, and ferrites. The effect of surface morphology, synthesis process, and various doping/composites on specific capacitance of supercapacitors were discussed in detail.

Introduction

The excess exhaustion of fossil fuels has raised great concern about global energy crisis as well as environmental pollution and demand the development of clean and renewable energy sources such as solar energy, wind energy, hydroenergy, and biomass [1]. The energy obtained from renewable sources has tremendous potential as an alternative to energy generated from conventional energy sources. The replacement of the traditional energy sources with clean and renewable energy is essential for continuous energy supply. However, the energy produced from these renewable energy sources depend on climatic conditions or geographical locations. These renewable energy sources need to be harvested when available and stored till required. Therefore, the development of high energy density energy storage systems is required to fulfill the energy needs around the world without any significant environmental impact.

Recently, energy storage devices such as rechargeable batteries, fuel cells, and supercapacitors have attracted significant attention, owing to their diverse applications in hybrid electric vehicles, energy management, and smart portable electronics [2–5]. Rechargeable batteries such as lithium-ion batteries

have been widely employed for various commercial application ranging from consumer electronics to hybrid electric vehicles. However, rechargeable batteries possess high energy density but often suffers from slow charging/discharging, limited cycle life, high cost of Li metal, low power density, poor cycle life, and environmental issues. Currently, supercapacitors are becoming more popular to overcome the issues raised by Li on rechargeable batteries such as low power density and limited cycle life [6].

Supercapacitors also known as electrochemical capacitors are important elements of modern energy storage technologies, owing to their notable properties such as higher energy density, prolonged stability, large cycle ability, and high power density as compared to batteries [7, 8]. Supercapacitors have superior properties as it provides high power density, fast charge/discharge rate, and long cycle life. Batteries are able to deliver energy density between 150–500 Whkg⁻¹ but have limited power densities due to slow electron and ion transport at high rates with discharge time more than 10 min [9, 10]. In contrast, supercapacitors, provide power output between 10–20 kWkg⁻¹ and release energy in less than 10 s [11, 12].

Meanwhile, the big challenge for the advancement in the field of supercapacitors is their low energy density [16, 17]. The comparison between performance parameters of batteries and supercapacitors is shown in Table 1. Moreover, due to their distinguished properties, supercapacitors have emerging applications that require fast on-off response such as wind power generation, photovoltaics, railways, hybrid electric vehicles, aerospace, portable, and wearable electronics [18, 19]. Supercapacitors are classified into two types on the basis of their charge storage mechanism, i.e., electrochemical double layer capacitors (EDLCs) and pseudocapacitors (PCs). EDLCs stores charge in strictly electrostatic manner by reversible ion adsorption at electrode interface, whereas energy storage mechanism for PCs is faradic redox reaction [20]. Hybrid supercapacitors, a combination of EDLCs and pseudocapacitors, are another type of supercapacitors and it utilizes the amalgamation of faradic and non-faradic mechanisms to store charges. There are many factors such as electrode material, electrolyte type, and operating potential windows that affects the performance of supercapacitor in terms of specific capacitance, cyclic stability, energy density, and power density. Out of these factors, the crucial one is the selection of electrode material that significantly affects the advancement in supercapacitor technology. The commercially fabricated supercapacitors often used carbon as electrode materials [21]. Carbon-based electrode materials store/release charges via physical adsorption/desorption of electrolytic ions on the surface of the electrode and this type of charge storage mechanism provide less than 10 Whkg⁻¹ energy density [22]. For practical utilizations, high energy density is always needed; therefore, so many efforts have been made in order to develop several other electrode materials with higher specific capacitance. The search of new electrode materials is always at top priority and a substantial challenge in order to reach the required supercapacitor performance.

Transition metal-based materials such as oxides, sulfide, selenides, nitrides, phosphide, and carbides can store much more energy than carbon due to faradaic charge transfer process in the electrochemical process [23, 24]. Due to their high theoretical specific capacitance (100–2200 Fg⁻¹), abundant sources, and low cost, transition metal oxides have attracted great attention of the researchers for supercapacitor applications [25]. Also, these materials possess multiple oxidation states due to which

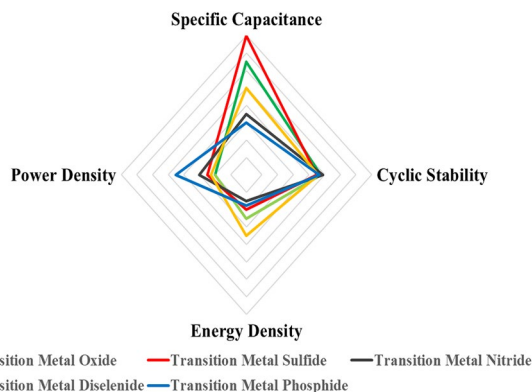


Figure 1: Radar plot of various characteristics of different transition metal-based supercapacitors.

multiple electrons transfer exists and discharge time extends, resulting in improving energy density in rapid Faraday redox reactions. In recent years, attention has been focused on various transition metal oxides such as MnO₂, RuO₂, transition metal hydroxides and their derivatives such as sulfides and selenides [26]. In addition to this, some transition metal hydroxides along with their derivatives such as Ni, Co, Cu, and Cd-based materials are often used to combine with capacitive electrode materials in order to assemble hybrid supercapacitor [27, 28]. These hybrid supercapacitors can attain high working potential and contribute to larger and fast charge storage capabilities and thus, considered as most promising materials for next generation supercapacitors. Various characteristics such as specific capacitance, energy density, power density, and cyclic ability of different transition metal-based supercapacitors are depicted in Fig. 1 via radar plot (Table 2).

It is evident that the key criteria for supercapacitors are rapid charge/discharge capability and long cycling stability of minimum 5,000 cycles. However, the low electrical conductivity, low power density, poor electrochemical stability, and several other issues still limit the transition metal-based materials for large-scale applications [29]. Recently, transition metals with nanoscale dimensions have aroused significant attention in numerous applications, owing to their attractive intrinsic characteristics, such as small size effect and surface effect [30, 31]. Compared with bulk materials, the combination of transition metals with carbon materials, conducting polymers, with

TABLE 1: Comparison between performance parameters of batteries and supercapacitors [13–15].

Performance parameters	Batteries	Supercapacitors		
			EDLC	TM
Charging/discharging	0.2–5 h	1–10 s	Moderate	High
Power density	< 1000 WKg ⁻¹	500–10,000 WKg ⁻¹	High	Moderate
Energy density	10–100 WhKg ⁻¹	1–10 WhKg ⁻¹	Low	High
Life cycle	500–1000 h	500,000 h	High	Low

introduction of lattice defects, heterostructures, metal heteroatoms, etc., are found to have improved electrochemical performance and thus valuable for the supercapacitor applications [32, 33]. Moreover, transition metal-based nanomaterials display large surface area and thus large amounts of surface electrons aggregate in the long-term charge/discharge process.

A large number of studies have drawn tremendous attention toward transition metal-based nanomaterials for supercapacitor applications. However, the deeper research is still necessary to understand the energy storage process and attenuation mechanisms. Additionally, the efficient discussion about the structure and design strategies, high power/energy densities, and fast pseudocapacitive reaction kinetics is demanded for the practical implementation of transition metal-based electrodes for supercapacitors. In this review, our prime focus is to summarize the recent advances in the field of transition metal-based nanomaterial electrodes for supercapacitors. Recent developments in the field of transition metal sulfides, selenides, oxides, ferrites, nitrides, and phosphides and their performance in terms of energy/power density, electrochemical stability, cyclic life have been discussed in detail. The review provides comprehensive overview of latest advancement in the various transition metal-based nanomaterials and their composites as well as recent methods to improve upon their rate capacities and cyclic performances from the year 2010 to present. Various strategies such as morphological control, interface and defect engineering, and composite fabrication for the enhancement in the electrochemical performances of the supercapacitors have been highlighted. More importantly, we discussed the challenges and perspectives of developing transition metal-based nanomaterials and their composites, along with the possible strategies and research directions to improve the electrochemical performances of electrode materials for advanced supercapacitors.

Transition metal oxides (TMO)

A good choice of electrode materials with remarkable electrical conductivity and a large specific surface area is an important factor for developing high-performance supercapacitors [34]. Transition metal oxide materials have been emerged as promising candidates to be used as electrodes of energy storage devices on account of their huge resources, easy synthesis procedure, eco-friendly nature, and other intriguing features such as large surface area, various morphologies, and high theoretical specific capacitance. Transition metal oxide materials have high specific capacitance (100–2000 Fg^{-1}) and higher energy density than carbon-based materials as well as better chemical stability than polymer materials [35, 36]. High energy and power density are the major requirement for wearable electronic equipment like flexible supercapacitors [37]. To enhance the capacitive behavior of supercapacitors, research community focused on

different transition metal oxides such as RuO_2 , ZnO , CoO , CuO , and NiO and their synthesis methods like hydrothermal [38], co-precipitation [39], microwave combustion method [40], and many more because of wide variety of structures and variable valences of TMOs.

Nwanya et al. deposited CuO films on indium tin oxide (ITO) substrate via successive ionic layer adsorption and reaction (SILAR) approach. The prepared material showed the good electrochemical performance which may be attributed to their nanosheet-like and nanorod-like morphology. It was found that nanosheet-like structure film showed specific capacitance of 566.33 Fg^{-1} [41]. Chaudhary et al. reported that doping of transition metals such as Co and Fe can significantly enhanced the electrochemical performance of copper oxide nanostructured-based supercapacitors. They synthesized pure, Co -doped, and Fe -doped CuO via simple co-precipitation method. They reported that Fe -doped CuO -based electrodes showed best electrochemical performances and the specific capacitance was obtained as 186 Fg^{-1} at 5 mVs^{-1} with retention rate of 90.47% after 5000 charge–discharge cycles. They reported that the high specific capacitance of Fe -doped CuO electrode was due to their nanorod-like morphology and the synergistic effect between Fe metal ion and CuO , which provided more reactive sites for electrochemical reactions [39].

It has been reported that the specific capacitance of transition metal ion-based electrodes can be improved by doping of TMO. Microwave irradiation method was used to synthesize ruthenium and cerium-doped tungsten oxide nanostructures by Paulraj and co-workers. They reported that small doping of transition metals like Ru and Ce can significantly improve the electrochemical performance of tungsten oxide material. The pure tungsten oxide nanostructures showed the specific capacitance of 13.9 Fg^{-1} at a current density of 0.1 Ag^{-1} , while 2 wt% Ru -doped and 2 wt% Ce -doped tungsten oxide material exhibited specific capacitances of 39.50 Fg^{-1} and 52 Fg^{-1} , respectively. The energy densities of pure, Ru -doped, and Ce -doped WO_3 were found to be 1.90, 5.49, and 7.22 Whkg^{-1} , respectively [42]. To get large operating potential window up to 1.6 V, Wang et al. prepared a flexible electrode based on MnO_2 carbonized cotton textile composite via chemical reaction method. The prepared electrode demonstrated highest capacitance of 751.78 Fg^{-1} at 1 mA.cm^{-2} with good cyclability of 98.7% after 10,000 cycles. The energy density and power density were found to be 5.71 mWhcm^{-3} and 3.97 Wcm^{-3} , respectively [43]. Cui et al. successfully synthesized MnO_2 nanoparticles on rGO /lignin-based porous carbon (RGO/PC) to form a ternary composite using electrodeposition method. The prepared ternary electrode showed the specific capacitance of 1136 mFcm^{-2} at a current density of 1 mAcm^{-2} and delivered energy density of $0.253 \text{ mWh.cm}^{-3}$ at 0.5 mAcm^{-2} and power density of 0.018 Wcm^{-3} at 5 mAcm^{-2} . They further reported

TABLE 2: Electrochemical performance of various transition metal-based materials compared with other existing literatures.

S. No	Electrode material	Synthesis method	Morphology	Electrochemical performance				References
				Specific capacitance	Cyclability	Power density (W.Kg ⁻¹)	Energy Density (Wh.Kg ⁻¹)	
1	NiSe ₂	Hydrothermal method	Hexapod-like	75 F g ⁻¹	5000 (94%)	–	–	[111]
2	NiSe ₂	Hydrothermal method	Mushroom-like	262 mAh g ⁻¹	8000 (83.4%)	–	–	[112]
3	MoSe ₂	Hydrothermal method	Nanosheets	16.25 F g ⁻¹	10,000 (87%)	7.5	–	[113]
4	N-rGO/NiSe ₂	Solvothermal method	Agglomerated	2451.4 F g ⁻¹	10,000 (85.1%)	841.5	40.5	[114]
5	PANI/CoSe ₂ /NF	Electrodeposition method	Ball-like	1980 F g ⁻¹	–	–	–	[115]
6	CoSe ₂ /rGO	Microwave method	Agglomerated	761 F g ⁻¹	10,000 (90%)	–	43.1	[116]
7	CoSe ₂ /NC	Selenylation	Nanosheets	120.2 mAh g ⁻¹	10,000 (92%)	–	–	[117]
8	WSe ₂ /rGO	Hydrothermal method	Nanosheets	389 F g ⁻¹	3000 (98.7%)	400	34.5	[118]
9	VSe ₂ /rGO	Hydrothermal method	Cuboid-like	680 F g ⁻¹	10,000 (81%)	3.3 kWkg ⁻¹	212	[119]
10	Ni ₃ S ₂	Hydrothermal method	Dendritic-like	626.1 Fg ⁻¹	2,000	–	–	[89]
11	Ni ₃ S ₄	Hydrothermal method	Microspheres	1796 Fg ⁻¹	1,000 (80.5%)	–	–	[91]
12	FeS ₂	Microwave assist method	Nano ellipsoid	515 Cg ⁻¹	5,000 (91%)	271.2	64	[95]
13	MnS	Self-template-etched method	Nanoplates	378 Fg ⁻¹	4,000 (90%)	–	–	[96]
14	NiCo ₂ S ₄ /NiS	Hydrothermal method	Nanospheres	1947.5 Fg ⁻¹	1,000 (90.3%)	160	43.7	[100]
15	NiCo ₂ S ₄ /AC	Sequential method	Onion-like	880 Fg ⁻¹	10,000 (87%)	1583	42.7	[101]
16	NiCo ₂ S ₄ @CoS ₂ @carbon cloth	Hydrothermal method	Nanostructures	1565 Fg ⁻¹	8,000 (90%)	242.8	17	[102]
17	MnS@rGO	Electrodeposition method	Sheet-like	2,220 Fg ⁻¹	1,000 (94.6%)	–	–	[106]
18	MnS@rGO@Ni-foam	Hydrothermal method	Nanosheet	150.3 mAhg ⁻¹	–	1,500	21.3	[107]
19	CrN/AC	Nitridation	Polyhedral	75 F/g	–	–	30 Wh.kg-1	[68]
20	CrN	OAMS	Triangular	17.7 mF cm ⁻²	92.2% (20,000 cycles)	18.2 Wcm ⁻³	7.4 mWh cm ⁻³	[70]
21	HfN film	DC magnetron	typical columnar structure	5.6 mF cm ⁻²	–	–	–	[72]
22	NbN	Magnetron sputtering	Dense grain	707.1 F cm ⁻³	92.2% (20,000 cycles)	–	–	[73]
23	VN/NCS	Nitridation	Sphere like	59F/g	–	801 W.Kg ⁻¹	19.8 Wh.Kg ⁻¹	[69]
24	CrN@NCs@CP	Magnetron sputtering	–	132.1 mF cm ⁻²	95.9% (20,000 cycles)	0.41 mW cm ⁻²	2.7 Wh kg ⁻¹	[76]
25	Fe ₂ N@OMC	Nanocasting with NH ₃ treatment	Homogeneous distribution	398 F/g	85% (1000 cycles)	–	–	[78]
26	NCF-N@FG/NF-3	Nitrogenization	–	2110 F/g	97.6% (5000 cycles)	7484.2 W/kg	56.3 Wh/kg	[80]

TABLE 2: (continued)

S. No	Electrode material	Synthesis method	Morphology	Electrochemical performance				References
				Specific capacitance	Cyclability	Power density (W.Kg ⁻¹)	Energy Density (Wh.Kg ⁻¹)	
27	Fe-doped CuO	Co-precipitation	Nanorod	186 F/g	90.47%(5000 cycles)	–	–	[39]
28	CuO thin film	SILAR	Nanosheet	566.33 F/g	–	–	–	[41]
29	α -Fe ₂ O ₃	LPD	Porous nature	960 F/g	–	–	–	[48]
30	MnO ₂ -based composite	Hydrothermal	–	751.78 F/g	98.7% (10,000 cycles)	3.97 W cm ⁻³	5.71 mWh cm ⁻³	[43]
31	Co ₃ O ₄ -SnO@SnO ₂	Hydrothermal	Nanosheet array	704F/g	91.5% (2000 cycles)	–	–	[38]
32	NiCo ₂ O ₄ @NiMoO ₄ /PANI/CC	Hydrothermal and polymerization	holothurian	1322.2 F/g	92.36% (5000 cycles)	443.2 W kg ⁻¹	90 Wh kg ⁻¹	[49]
33	Ru compound	Chemical route	Agglomerated particles	797.7 F/g	90.2% (2000 cycles)	50 W/Kg	17.3Wh/Kg	[46]
34	Ce-doped WO ₃	Microwave irradiation method	Agglomerated particles	52 F/g	–	–	7.22 Wh/Kg	[42]
35	Co ₂ P	Microwave-assisted hydrothermal treatment	Nanoshuttles	246 Fg ⁻¹	72% (1000 cycles)	–	–	[124]
36	CoP	Hydrothermal method followed by Phosphidation	Nanowire	571.3 mFcm ⁻²	82% (5000 cycles)	114.2 mWcm ⁻³	0.69 mWh/cm ⁻³	[125]
37	Mn-doped CoP	Hydrothermal Method	Nanosheet-Nanowire cluster arrays	8.66 F cm ⁻²	–	193 W Kg ⁻¹	35.21Wh Kg ⁻¹	[126]
38	Cu ₃ P	Direct electro-oxidation and phosphidation	Nanotube arrays	300.9 F g ⁻¹	81.9% (5000 cycles)	17,045.7 W kg ⁻¹	44.6 W h kg ⁻¹	[123]
39	Ni-Co-P	Hydrothermal method followed by phosphorization	Nanowire	1395 F g ⁻¹	83.04% (20,000 cycles)	46.53 kW kg ⁻¹	53.31 W h kg ⁻¹	[128]
40	Ni-Fe-P	Hydrothermal method followed by Phosphidation	Nanosheet	1358 C g ⁻¹	91.5% (10,000 cycles)	800 W kg ⁻¹	50.2 Wh kg ⁻¹	[129]
41	Zn-Ni-P	Hydrothermal method followed by phosphorization	Nanosheet arrays	384 mAh g ⁻¹	93.05% (20,000 cycles)	611 W kg ⁻¹	90.12 Wh kg ⁻¹	[130]
42	Mn-Ni-Co-P	Electrodeposition method followed by low-temperature PH ₃ plasma treatment	Nanoflower	1690 C g ⁻¹	97.4% (4500 cycles)	749.91 W kg ⁻¹	55.25 Wh kg ⁻¹	[131]

TABLE 2: (continued)

S. No	Electrode material	Synthesis method	Morphology	Electrochemical performance				References
				Specific capacitance	Cyclability	Power density (W.Kg ⁻¹)	Energy Density (Wh.Kg ⁻¹)	
43	NiFe ₂ O ₄	Solvothermal Method	Spherical	368 F g ⁻¹	88% (10,000 cycles)	225.8 W kg ⁻¹	10.4 Wh kg ⁻¹	[161]
44	MnFe ₂ O ₄	Co-precipitation method	Spherical	173 F g ⁻¹	105% (10,000 cycles)	1207 W kg ⁻¹	12.6 Wh kg ⁻¹	[156]
45	ZnFe ₂ O ₄	Ultrasonic irradiation technique	Spherical	712 F g ⁻¹	96.6% (2000 cycles)	250 W kg ⁻¹	24.2 Wh kg ⁻¹	[157]
46	CuFe ₂ O ₄	Solvothermal method	Spherical	189.2 F g ⁻¹	84% (1000 cycles)	–	–	[158]
47	CoFe ₂ O ₄	Hydrothermal process	Nanoplatelets (square-shaped nanoparticles)	429 F g ⁻¹	98.8% (6000 cycles)	–	10.68 Wh kg ⁻¹	[159]
48	Ce _{0.5} Co ₂ Fe _{1.5} O ₄	Hydrothermal method	Spherical grain nanoparticles	937.50 F g ⁻¹	82.3% (10,000 cycles)	–	–	[160]
49	Ni _{0.5} Zn _{0.5} Fe ₂ O ₄	Hydrothermal method	Thin hexagonal platelets	504 F g ⁻¹	93.05% (20,000 cycle)	450 kW kg ⁻¹	56 kWh kg ⁻¹	[163]
50	CuCoFe ₂ O ₄	Self-combustion method	Spherical	220 F g ⁻¹	–	605 W kg ⁻¹	34.7 Wh kg ⁻¹	[162]

that MnO₂ nanoparticles possessed nanoflake-like morphology which after interconnection formed a porous structure due to which more specific area was provided to active material for the intercalation process [44]. In a report, sol-gel method was used to fabricate a distinctive flexible electrode based on ZnO/rGO/ZnO free-standing sandwich-type material. According to this study, graphene oxide was used as a substrate for deposition of ZnO films. The specific capacitance of prepared electrode was reported as 60.63 Fg⁻¹ at scan rate of 5 mVs⁻¹[45]. Wang et al. synthesized SnO₂nanosheets on carbon cloth by using simple hydrothermal method and then annealed under argon atmosphere to get composite of SnO@SnO₂. To improve the specific capacitance and cycle stability, Co₃O₄ was added to SnO@SnO₂ skeleton to prepare a hierarchical nanostructured composite Co₃O₄-SnO@SnO₂. The specific capacitance of prepared composite electrode was reported to be 1.056 Fcm⁻² at 1 mAcm⁻² with excellent stability of 91.5% after 2000 cycles [Fig. 1(a)–(c)][38]. Guo et al. prepared a ruthenium-based nanohybrid compound comprised of ruthenium nanoparticles capped by cysteine and hydrous ruthenium oxide (RuO₂·H₂O). It was reported that Ru-based compound exhibited great specific capacitance of 797.7 Fg⁻¹ at the scan rate of 0.01 Vs⁻¹, while RuO₂·H₂O and Ru nanoparticles possessed specific capacitances of 231.1 Fg⁻¹ and 134.0 Fg⁻¹, respectively, at the scan rate of 0.01 Vs⁻¹. Ruthenium compound retained its initial capacitance of 90.2% after 2000 cycles and showed the better electrochemical stability as compared to hydrous ruthenium oxide and Ru nanoparticles. Among all these three electrodes, Ru compound

also attained maximum energy density of 17.3Whkg⁻¹, while RuO₂·H₂O and Ru nanoparticles possessed energy densities of 4.93 and 2.11 Whkg⁻¹, respectively. The improved electrochemical performance of ruthenium compound were because of the synergistic effect, which facilitated the electron-proton transfer process. [46]. Huang et al. successfully fabricated the flexible microsupercapacitor by depositing platinum thin films and hydrous ruthenium oxide on polyethylene terephthalate (PET) sheet. The prepared supercapacitor exhibited great energy storage capacity along with power density of 73,460 mWcm⁻³ and energy density of 24.9 mWhcm⁻³[47]. Khatavkar et al. deposited α-Fe₂O₃ on thin and flexible stainless steel mesh substrate via liquid phase deposition technique. From galvanic charge-discharge (GCD) curves, the highest specific capacitance was calculated to be 960 Fg⁻¹ at 4 mA cm⁻², while from cyclic voltammetry (CV) curve, the specific capacitance was obtained to be 548 Fg⁻¹ at 5mVs⁻¹[48]. The improved specific capacitance was reported due to the synergistic effect between the components. Shen et al. successfully grown the nanowire arrays of NiCo₂O₄ on carbon cloth by hydrothermal method with annealing process. By following the same procedure, NiMoO₄nanosheets were grown on NiCo₂O₄. At last, in situ polymerization was used to coat the surface of NiCo₂O₄@NiMoO₄ arrays with polyaniline (PANI) nanorods to get NiCo₂O₄@NiMoO₄/PANI/CC. The prepared composite revealed holothurian-like morphology [Fig. 1(d), (e)], which provide better electrochemical transportation of ions within the electrolyte. The specific areal capacitance of prepared composite electrode was found to be 1322.2 Fg⁻¹ at

current density 1.0 mAcm^{-2} with retention rate of 92.36% after 5000 cycles [Fig. 1(f)]. The maximum energy and power densities were found to be 90 Whkg^{-1} and 443.2 Wkg^{-1} , respectively [49].

Liu et al. prepared a hybrid structure of phosphorous-doped Co_3O_4 nanoparticles in situ inserted into phosphorous and nitrogen co-doped carbon nanowires by following pyrolysis-oxidation-phosphorization strategy. The prepared hybrid structure maintained 1D-oriented arrangement, which exhibited a large surface area due to hierarchically porous structure and enabled sufficient diffusion and transfer of electrolyte ions. It was reported that the fabricated hybrid P- Co_3O_4 @P, N-C delivered the highest specific capacity of 669 mCcm^{-2} at 1 mAcm^{-2} with good cyclability and also achieved a high energy density of 47.6 Whkg^{-1} at 750 Wkg^{-1} [50]. Li et al. synthesized Co_3O_4 /NiCoAl-layered double hydroxide nanowire arrays by using simple hydrothermal method. They reported that layered double hydroxide nanosheets provided large electroactive surface area and were uniformly distributed on Co_3O_4 nanowires which allowed fast electron transport and enhanced the electrochemical performance of prepared material [51]. Recently, Lee et al. reported that cobalt-vanadium-layered double hydroxides could become a good candidate as an electrode for hybrid supercapacitors. To enhance the charge storage mechanism, they controlled the molar ratio of vanadium and cobalt. It was noticed that prepared electrode exhibited highest specific capacitance of 1579 Fg^{-1} at 1 Ag^{-1} . The prepared electrode also possessed highest energy density of 75.71 Whkg^{-1} at a power density 1043.72 Wkg^{-1} with cyclic stability 82% after 1000 cycles [52]. Shinde et al. used a combination of chemical deposition strategies to synthesize multicomponent CoMn_2O_4 @NiCo-OH and VN@NC nanostructures on carbon cloth. The prepared electrode showed high specific capacity of $349.0 \text{ mA h g}^{-1}$ at 1 mA cm^{-2} with good cyclic stability. The fabricated device demonstrated maximum specific energy of 68.83 Whkg^{-1} at a specific power of 2048 Wkg^{-1} [53].

Transition metal nitrides (TMN)

Transition metal nitrides are emerging as unprecedented electrode materials for energy storage devices involving supercapacitors, lithium-ion batteries, lithium-ion hybrid capacitors, and lithium-sulfur batteries because of their unique electronic structure, superior chemical stability, high conductivity and excellent catalytic activity [54]. Generally, TMNs have a special combination of several properties such as metallic, ionic, and covalent [55, 56]. Incorporation of nitrogen atoms can change the density of state in the d-band. The less shortage in d-band occupation and high density of states of metal near the Fermi level improves the electron donating ability of metal nitrides which is responsible of improved electrochemical properties and

noble metal-like activities to TMNs [57]. TMNs have higher volumetric densities compared to carbon-based materials (generally $< 1.0 \text{ g cm}^{-3}$). For example, the volumetric density of NbN [58], VN [59], TiN [58], MoN [60], and WN is 8.47 g cm^{-3} , 6.13 g cm^{-3} , 5.4 g cm^{-3} , 9.2 g cm^{-3} , and 17.7 g cm^{-3} , respectively [57]. Because of high volumetric densities, TMNs offer high volumetric energy density [59]. Transition metal nitrides are the interstitial compounds of group IVB-VIB in which the nitrogen atoms are incorporated into the interstitial sites of the parent metals [61].

Synthesis procedure of TMNs also plays an important role toward the electrochemical performances of TMNs [59]. The formation of nitrides undergoes some issues because of the thermodynamic barrier in nitride formation that involves the formation and deformation of triple bond between nitrogen atoms. Various synthesis methods to synthesize TMNs have been discussed in literature. Some of the methods are sol-gel, co-precipitation, hydrothermal, and sonochemical [58, 62]. TMNs such as vanadium nitride (VN), titanium nitride (TiN), niobium nitride (Nb_4N_5 or NbN), and molybdenum nitride (MoN or Mo_2N), with different morphologies including nanoparticles (NPs), nanorods (NRs), nanowires (NWs), nanotubes (NTs), nanosheets (NSs), and nanohybrids were synthesized and used for supercapacitor applications [58, 59, 63–67]. Das et al. prepared the nitride nanoparticles of chromium and cobalt by simple nitridation of their corresponding metal oxides at relatively low temperature, in the presence of ammonia and oxygen. The particle size of synthesized nanoparticles was found in the range of ~ 20 – 30 nm . CrN nanoparticles showed polyhedral morphology, while agglomeration of particles was observed in CoN nanoparticles. In this study, the specific capacitances of CrN/AC and CoN/AC were found to be 75 Fg^{-1} and 37 Fg^{-1} , respectively, at a current density of 30 mA g^{-1} [68].

Jiang et al. prepared vanadium nitride and nitrogen-doped carbon hollow sphere nanocomposite by simple nitridation of corresponding oxide precursor ($\text{V}_2\text{O}_3/\text{C}$). The prepared composite showed excellent energy density of 19.8 Whkg^{-1} at a power density of 801 Wkg^{-1} [69]. Qi et al. employed oblique angle magnetron sputtering (OAMS) to fabricate nanostructured porous CrN thin films for supercapacitor applications as shown in Fig. 2(a). It was found that OAMS-deposited CrN film showed the specific capacitance of 17.7 mFcm^{-2} at 1.0 mAcm^{-2} , which was eight times greater than normal magnetron sputtered (NMS) film [Fig. 2(b)–(d)]. It was also observed that OAMS-deposited CrN film electrodes exhibited maximum power and energy densities of 18.2 Wcm^{-3} and 7.4 mWhcm^{-3} , respectively [70]. It was reported that the specific capacitances of nitride films can be enhanced by silicon nanowire arrays coated with chromium. Guerra et al. deposited CrN films on Si nanowires via magnetron sputtering method. They reported the highest areal capacitance of prepared 3D electrode as 1806 mFcm^{-2} at

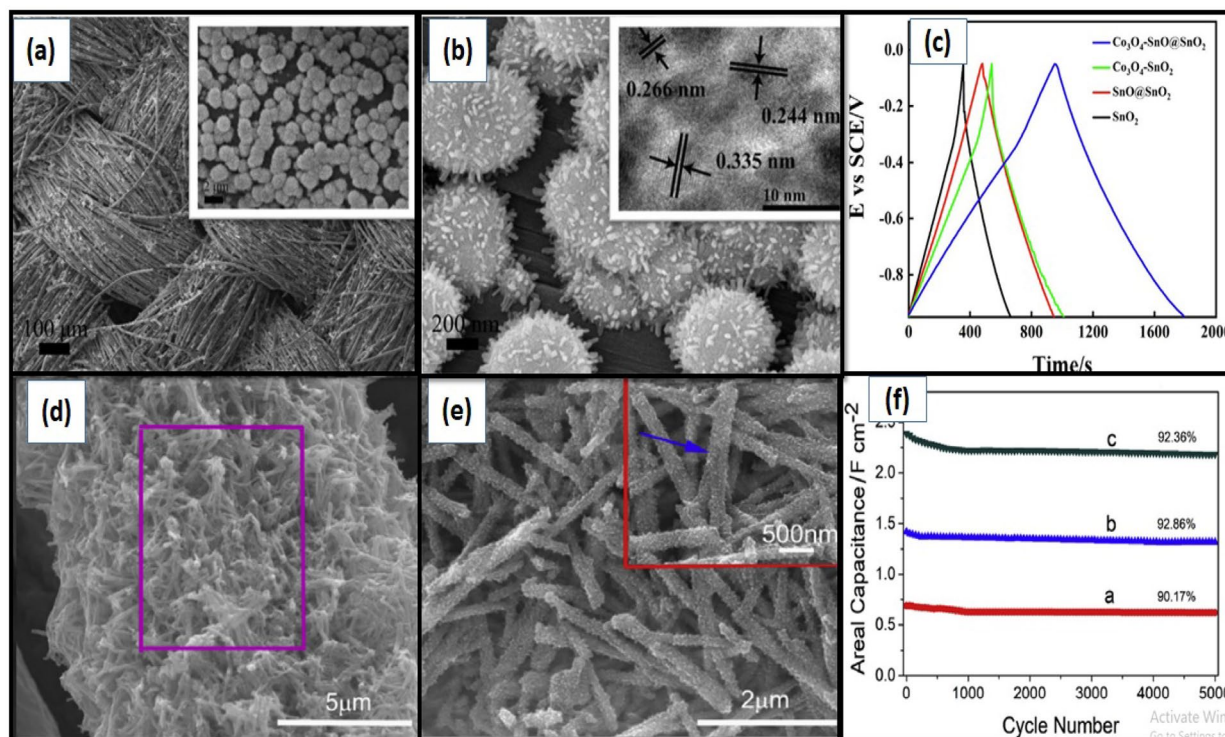


Figure 2: (a, b) SEM images of $\text{Co}_3\text{O}_4\text{-SnO@SnO}_2$, (c) GCD curves of SnO_2 , SnO@SnO_2 , $\text{Co}_3\text{O}_4\text{-SnO}_2$, $\text{Co}_3\text{O}_4\text{-SnO@SnO}_2$ electrodes at 1 mA cm^{-2} . (Reprinted with permission from ref. [38]) (d & e) SEM morphologies of $\text{NiCo}_2\text{O}_4\text{@NiMoO}_4\text{/PANI/CC}$ composite at different magnification, (f) curve between capacitance retention and charge/discharge cycle number of $\text{NiCo}_2\text{O}_4\text{/CC}$ (a), $\text{NiCo}_2\text{O}_4\text{@NiMoO}_4\text{/CC}$ (b), and $\text{NiCo}_2\text{O}_4\text{@NiMoO}_4\text{/PANI/CC}$ (c) at 0.1 mA cm^{-2} current density. (Reprinted with permission from ref. [49]).

a scan rate of 5 mVs^{-1} , with retention rate of 92% after 15,000 cycles [71].

It was reported that the surface roughness of films can be significantly improved after etching process without change in phase structure. Gao et al. deposited HfN films by DC magnetron sputtering and then after deposition, etching process was done on the surface of films in the presence of plasma. Etching process reduced the charge transfer resistance of the films and increased the specific capacitance of the films eight times than that of the film without etching. It was reported that plasma-etched film attained high capacitance of 5.6 mFcm^{-2} at $1.0 \text{ mA}\cdot\text{cm}^{-2}$ with excellent cyclic stability, which make it suitable for electrode materials in supercapacitors [72]. According to Shen et al., reactive magnetron sputtered niobium nitride (NbN) thin film could also become the good electrode material for supercapacitors as the volumetric capacitance of NbN thin film electrode was found to be 707.1 Fcm^{-3} at 1 mAcm^{-2} with cyclic stability of 92.2% after 20,000 cycles [73]. He et al. reported the synthesis of Mo_2N with polyaniline that can be used as an electrode material in a supercapacitor. The prepared composite material ($\text{Mo}_2\text{N@PANI}$) showed higher specific capacitance of 111.8 Fg^{-1} at the current density at 0.5 Ag^{-1} with higher rate performance of 66.4% [74]. Ouendi et al. fabricated tungsten nitride films on silicon wafer via reactive

magnetron sputtering. It was noticed that the best performance of prepared films was achieved at room temperature rather than higher temperatures. W_2N film displayed areal capacitance as 550 mFcm^{-2} and volumetric capacitance greater than 700 Fcm^{-3} which confirmed the pseudocapacitive nature of these films [75].

Recently, Xu et al. deposited 3D porous chromium nitride films on MOF-derived nitrogen-doped nanosheet on carbon paper (CrN@NCs@CP) by magnetron sputtering technique. SEM morphology of the prepared composite revealed the large surface area that facilitates the diffusions of electrolytes. The specific capacitance of prepared composite electrode was observed to be 132.1 mFcm^{-2} at current density of 1.0 mAcm^{-2} with capacitance retention of 95.9% after 20,000 GCD cycles [76]. A new type of vanadium-based V_2NT_x ($T_x = \text{F, O}$ as surface terminating groups) composite was prepared by Venkateshalu et al. via etching process of Al layer from V_2AlN precursor. It was found that V_2NT_x electrode showed a high power density of 3748.4 Wkg^{-1} and energy density of 15.66 Whkg^{-1} . They reported that the specific capacitance of V_2NT_x electrode was 113 Fg^{-1} at the current density of 1.85 mA cm^{-2} , with excellent capacitance retention of 96% after 10,000 cycles [77].

Xu and co-workers prepared a composite of iron nitride and ordered mesoporous carbon ($\text{Fe}_2\text{N@OMC-2}$) by nanocasting

method along with ammonia calcination. The morphology of the as-synthesized electrode was observed to homogeneously dispersed. This composite was used as a negative electrode material for supercapacitors, which showed impressive specific capacitance of 547 Fg^{-1} at 1 mVs^{-1} with capacitance retention of 85%. The capacitance of prepared composite was found to be two times higher than bare iron nitride sample. It was reported that OMC significantly enhanced the electrochemical performance of bare Fe_2N because it provided more active sites [78]. To achieve excellent capacitance of 507 Fg^{-1} at 0.5 Ag^{-1} , a composite of Fe_2N @activated carbon was prepared via hydrothermal method by Sliwak and co-workers. It was noticed in this study that carbon material supported the bare material to increase the porosity. The great capacitance was achieved by good pseudocapacitance of iron nitride material and porous behavior of activated carbon [79]. Ishaq et al. prepared a hybrid electrode of nickel–cobalt–iron nitride nanoparticles on Ni-foam supported with fluorinated graphene by using thermal nitrogenization treatment. The prepared electrode demonstrated specific capacitance of 2110 Fg^{-1} at 1 Ag^{-1} with capacitance retention of 97.6% after 5000 cycles. They used the as-synthesized material as electrode in supercapacitors because it exhibited high energy density of 56.3 Wh/kg at 374.6 W/kg and power density of 7484.2 Wkg^{-1} at 39.5 Whkg^{-1} [80]. Ouldhamadouche et al. used a DC magnetron technique to prepare a composite of vanadium nitride and CNT which showed the 3D nanotree-like morphology. The electrochemical study of the prepared composite revealed the high areal capacitance of 37.5 mFcm^{-2} at a scan rate of 2 mVs^{-1} [81]. Zhang et al. synthesized a composite electrode of vanadium nitride and carbon via simple adsorption of VO^{3-} . At the current density of 0.5 Ag^{-1} , the specific capacitance of prepared electrode was reported to be 260 Fg^{-1} and the capacitance retention was reported to be 91.1% after 1000 cycles. The energy and power density delivered by prepared composite was found to be 40.5 Whkg^{-1} and 3760.7 Wkg^{-1} , respectively [82]. To achieve a better electrochemical performance, Salman and co-workers fabricated a hybrid of tungsten nitride and reduced graphene fiber. The hybrid material electrode showed the specific capacitance of 16.29 Fcm^{-3} at 0.05 Acm^{-3} , which is higher than individual reduced graphene oxide fiber as well as tungsten oxide/rGO. The capacitance retention rate of nitride-based hybrid electrode was noted to be 87% after 10,000 cycles [83].

Transition metal sulfide (TMS)

Transition metal sulfides like MoS, CoS, NiS, MnS, FeS, etc., have attracted tremendous interest as potential electrode materials for electrochemical cells due to their high specific capacity, low cost, high abundance, and stress-free production [84, 85]. The electrochemical characteristic of transition metal sulfides is much better than the transition metal oxides. Hence, the use of

sulfur instead of oxygen as an element with lower electronegativity increases performance compared to transition metal oxides [86, 87]. The unique properties of transition metal sulfides are related to their specific forms and structures with exceptional surface morphology, exhibiting unique shapes such as nano-flowers, nanorods, nanowires, nanohoneycomb like results their extraordinary electrical performance [88].

It was reported that dendritic crystal structures were found to be suitable for supercapacitor applications because of their widespread structure in which they have a stem and many side branches grow out with primary, secondary, tertiary, and even high-order branches. These structures provide a large specific surface area and short diffusion path for electrons and ions, result enhancing their electrochemical properties. Keeping this in view, Zhang et al. studied a hierarchical three-dimensional (3D) Ni_3S_2 dendritic structure as a supercapacitor electrode material using 1 M KOH as an electrolyte. They have synthesized three nickel sulfides via hydrothermal method at various temperatures. Schematic illustration of the formation process of Ni_3S_2 3D hierarchical dendrites can be seen from Fig. 3(a). They mentioned three nickel sulfides as Ni_3S_2 -120, Ni_3S_2 -150 and Ni_3S_2 -180. Figure 3(b) represents the surface morphology of 3D dendritic Ni_3S_2 , synthesized via hydrothermal at 120°C over 6 h. The obtained 3D network structure provided more active sites as well as facilitated the ion charge transfer. They reported that the length of the dendrite decreases as the reaction temperature increases and thickness increases upon increasing reaction time. The Ni_3S_2 -120 samples were found to have the largest specific capacitance of 626.1 Fg^{-1} at 5 Ag^{-1} and was stable, even after 2,000 cycles [Fig. 3(c), (d)] [89].

Kim et al. fabricated Ni_3S_2 electrodes for supercapacitor applications via electrodeposition of Ni_3S_2 on a Ni surface using 3 M NaCl as an electrolyte. The resulting Ni_3S_2 samples were found to have the specific capacitance of 786.5 C g^{-1} at a current density of 10 mA cm^{-2} with cycling stability of 93.9% even after 6,000 cycles [90]. It was reported that the electrochemical properties depend on porosity and surface area of the materials because high porosity and high specific surface area provide more electroactive sites, resulting in better ion transportation for electrochemical reactions. Chen et al. used a one-pot hydrothermal method to synthesize a new 2D/3D/ $\text{Ni}/\text{Ni}_3\text{S}_4$ composite in which 3D microspheres progressively grew in or were secured by interconnected 2D nanosheets. The obtained composite possesses high specific surface and unique interconnected 2D structure which provided more active sites as well as highway for electron transfer. It was observed that the composite had a high specific capacitance of $1,796 \text{ Fg}^{-1}$ at a current density of 1 Ag^{-1} , and retained 80.5% of its initial capacitance even after 1,000 charge/discharge cycles [91]. Several nanostructured electrode materials based on CoS have been developed for energy storage and supercapacitors applications [92]. It was reported that

synthesized porous and hollow CoS_2 nanocubes can be used for supercapacitor applications because of their high specific surface area ($113.9 \text{ m}^2 \text{ g}^{-1}$) and mesoporous structure with the average pore size of 6.3278 nm . The as-prepared CoS_2 hollow nanocubes showed high specific capacitance of 936 F g^{-1} at a current density of 1 A g^{-1} , with good cycling stability of 83% even after 5,000 cycles at 5 A g^{-1} [93]. Jia et al. synthesized quadruple-shelled hollow CoS_2 dodecahedrons via two-step process. First, they prepared uniform yolk-shell Co_3O_4 dodecahedron from zeolitic imidazolate framework-67 and then they did sulfuration of Co_3O_4 with sulfur powder to obtain quadruple-shelled CoS_2 hollow dodecahedrons. This type of structure provided short ions and electron diffusion length balanced the electrolyte utilization which enhanced the structural stability. It was reported that the resulting sample have surface area of $51.8 \text{ m}^2 \text{ g}^{-1}$ and high specific capacitance of 375.2 F g^{-1} with significant retention rate [94]. FeS_2 nanoellipsoid for supercapacitor applications were synthesized via simple microwave assist method. The obtained nanoellipsoid morphology was beneficial to enhance the surface area of FeS_2 which provided more active sites for electrochemical reactions. It was reported that FeS_2 electrodes possesses wide working potential ranging -1.2 to 0 V and fairly high SCs of 515 C g^{-1} and 355 C g^{-1} at current densities of 1 A g^{-1} and 20 A g^{-1} , respectively, with high energy density of 64 Wh kg^{-1} at 271.2 W kg^{-1} and 91% of its original capacity retention even after 5,000 cycles [95]. Deli and co-workers used $\text{Mn}_3[\text{Fe}(\text{CN})_6]_2$ microcubes as a template and Mn source to

synthesize two-dimensional MnS nanoplates via self-template-etched method. The as-prepared $\gamma\text{-MnS}$ showed 2D nanoplate-like morphology and delivered good specific capacitance of 378 F g^{-1} at a current density of 0.2 A g^{-1} , with 90% retention of their capacitance even after 4,000 cycles at 1.0 A g^{-1} . The improved electrochemical performances were reported due to the special 2D structure, as 2D $\gamma\text{-MnS}$ nanoplate possess higher electron conductivity and charge transfer ability [96].

Several investigations have been carried out to improve the electrochemical activities of tin sulfides (SnS and SnS_2) using variety of approaches. These include metal or non-metal ion doping, the use of carbon matrices, and material engineering of nanostructured forms of tin sulfide, and their nanocomposites [97]. Parveen et al. recently synthesized SnS_2 in a variety of forms, including ellipsoid-like tin sulfide, flower-like tin sulfide and sheet-like tin sulfide via solvothermal method using different types of solvents. It was observed that flower-like tin sulfide has better capacitive performance which means that the morphology has significant effect on the electrochemical reaction. It was noticed that flower-like SnS_2 have higher surface area because of its small pore size and provided more active sites for the intercalation of ions, resulting in a high specific capacitance of 432 F g^{-1} at current density of 1 A g^{-1} . Various SnS_2 nanostructures were reported to have good cycling stability at 5 A g^{-1} with capacitance retention of 90%, 82%, and 80% for the flower-like SnS_2 , ellipsoid-like SnS_2 , and sheet-like SnS_2 , respectively, even after 2,000 cycles [98].

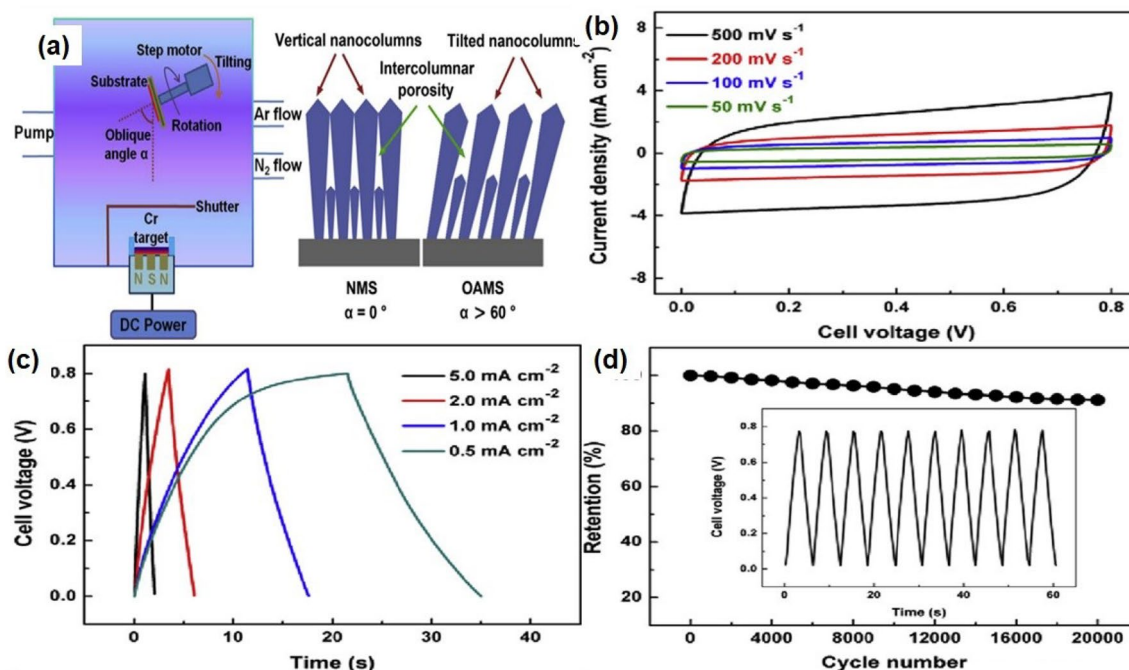


Figure 3: (a) Schematic representation of NMS and OAMS techniques and microstructure of as-deposited thin films, (b) CV curves at various scan rates, (c) GCD curves at various current densities, (d) Cycling performance at a current density of 2.0 mA cm^{-2} for 20,000 cycles with first 10 cycles of charge-discharge curves (inset). (Reprinted with permission from ref. [70]).

It was reported that mixed metal sulfides (MMSs) and hybrid metal sulfides (HMSs) have larger electrochemical capacitances than non-metallic sulfides, because of their strong electrochemical redox potentials and superior electronic conductivity. Yu and co-workers have synthesized a mixed metal sulfide (NiCo_2S_4) for hybrid supercapacitors (HSCs). They reported that NiCo_2S_4 had a substantially higher specific capacitance than the non-metallic sulfides NiS and CoS. The electrical conductivity of NiCo_2S_4 was reported to be around 100 times as of NiCo_2O_4 [99]. Xu et al. reported that the $\text{NiCo}_2\text{S}_4/\text{NiS}$ hollow nanospheres nanocomposite were grown directly on the nickel foam via simple hydrothermal method. The obtained unique hollow nanosphere enhanced the specific area, improved productivity, and provided more electroactive sites. They used $\text{NiCo}_2\text{S}_4/\text{NiS}$ hollow nanospheres as positive electrodes and the porous activated carbon as negative electrode to make an asymmetric supercapacitor, the $\text{NiCo}_2\text{S}_4/\text{NiS}$ electrode exhibits an outstanding specific capacitance of 1947.5 Fg^{-1} at 3 mA cm^{-2} [100]. Guan et al. [101] described the synthesis of onion-like NiCo_2S_4 with hollow structured shells via a sequential exchange method. They first transformed onion-like Co_3O_4 particles into onion-like Co_4S_3 particles with hollow structured shells by an anion-exchange reaction between Co_3O_4 and S_2 ions; afterward these onion-like Co_4S_3 particles converted into NiCo_2S_4 particles via a second cation-exchange reaction with Ni^{2+} ions. It was observed that the onion-like NiCo_2S_4 sample have multi-shelled structure with each shell being hollow. This type of seven-layered onion-like structure was believed to be more structurally stable which was beneficial for the enhanced electrochemical stability for supercapacitors. The resulted onion-like NiCo_2S_4 /activated carbon sample exhibited high energy density of 42.7 Whkg^{-1} at a power density of 1583 Wkg^{-1} , with good cycling stability of 87% even after 10,000 cycles at a current density of 10 Ag^{-1} . Govindasamy et al. fabricated hybrid $\text{NiCo}_2\text{S}_4/\text{CoS}_2$ nanostructures on a piece of carbon cloth via hydrothermal method [Fig. 4(a)]. It was concluded from the surface morphology of $\text{NiCo}_2\text{S}_4/\text{CoS}_2$ on carbon cloth that NiCo_2S_4 ultrathin nanosheets cover CoS_2 nanowires, resulting in 3D interconnected porous network. This type of porous network allowed facile electrolyte ion access for fast and reversible redox reactions. It was observed that the prepared $\text{NiCo}_2\text{S}_4/\text{CoS}_2$ have a strong specific capacitance of 1565 Fg^{-1} at a current density of 1 Ag^{-1} [Fig. 4(b), (c)], with 91% specific capacitance retention even after 8000 cycles as displayed in Fig. 4(d). Also, the maximum energy density was found to be as 17 Whkg^{-1} at a power density of 242.8 Wkg^{-1} [102].

Iron sulfide is inexpensive, exhibits very good electrical conductivity, and has an excessive active site. Iron sulfide (FeS_2) has attracted the attention of numerous researchers for its potential use in energy storage applications [103]. Several different forms of FeS_2 -based composites with various interesting morphologies and structures have been prepared for super

capacitor applications. It was reported that the electrochemical performances of pure metal sulfides can be improved by making its hybrid material with rGO. It may be due to improved electrical conductivity, high surface area, and enhanced electron and ion transfer mechanism of the hybrid materials compared to their pure form. Balakrishnan and co-workers synthesized hybrid microsphere of FeS_2 and reduced graphene oxide (rGO) via superficial hydrothermal method for supercapacitor applications. The obtained rGO- FeS_2 hybrid material possess better electrochemical performance due to the synergetic effects of the higher active surface area of rGO and the redox property of the FeS_2 microspheres. The specific capacitance of hybrid material was reported as 112.41 mFcm^{-2} , with specific capacitance retention of 90% after 10,000 cycles, which was substantially much higher than that of pure iron sulfide (70.98 mFcm^{-2}) at 5 mVs^{-1} [104]. Zardkhoshoui et al. used a simple hydrothermal method for the synthesis of graphene wrapped NiCo_2Se_4 microspheres and petal-like FeS_2 on a nickel foam substrate. The specific surface area of the graphene wrapped NiCo_2Se_4 microspheres sample was estimated to be around $75.5 \text{ m}^2\text{g}^{-1}$. They reported that the resulting petal-like FeS_2 with unique structure and highly porous texture exhibited maximum specific capacitance of 321.30 Fg^{-1} at 2 Ag^{-1} . They also used graphene wrapped NiCo_2Se_4 as the positive electrode and petal-like FeS_2 as the negative electrode to create a flexible and an asymmetric solid supercapacitor, which showed maximum specific capacitance of 2112.30 Fg^{-1} at 1 Ag^{-1} and its energy density was reported as 78.68 Whkg^{-1} [105]. Naveen et al. coated Ni-foam with 0.2 mg reduced graphene oxide (rGO) via dip coating method and then used rGO coated Ni-foam for electrodeposition of MnS. It was observed that the electrodeposited $\text{MnS}/\text{rGO}/\text{Ni}$ -foam composite showed a high specific capacitance of $2,220 \text{ Fg}^{-1}$ at 0.5 Ag^{-1} , with good cycling stability of 94.6% even after 1,000 cycles at 20 Ag^{-1} [106]. Xu et al. synthesize MnS/rGO composite via simultaneous growth of MnS and reduced graphene oxide (RGO) on Ni-foam ($\text{MnS}/\text{rGO}/\text{Ni}$ -foam) using one-pot hydrothermal method. They used $\text{MnS}/\text{rGO}/\text{Ni}$ -foam as positive electrode and activated carbon (AC) generated from walnut shells as negative electrode to create $\text{MnS}/\text{rGO}/\text{Ni}$ -foam/AC hybrid supercapacitor, which exhibit maximum energy density of 37.9 Whkg^{-1} and a maximum power density of $1,500 \text{ Wkg}^{-1}$ and retain the energy density of 21.3 Whkg^{-1} at a high power density of 3750 Wkg^{-1} [107]. Rasmita et al. synthesized stannous sulfide (SnS) nanoparticles via hydrothermal method and later stannous sulfide-carbon black (CB) composite via milling process. They found that the electrochemical performance was increased when carbon black was combined with SnS in the ratio of 4:1 (SnS:CB). The resulting sample SnS-CB (carbon black) exhibited maximum specific capacitance of 201 Fg^{-1} with cycling stability of 88% even after 1,000 cycles. The resulting sample suggested that the stannous sulfide with carbon black

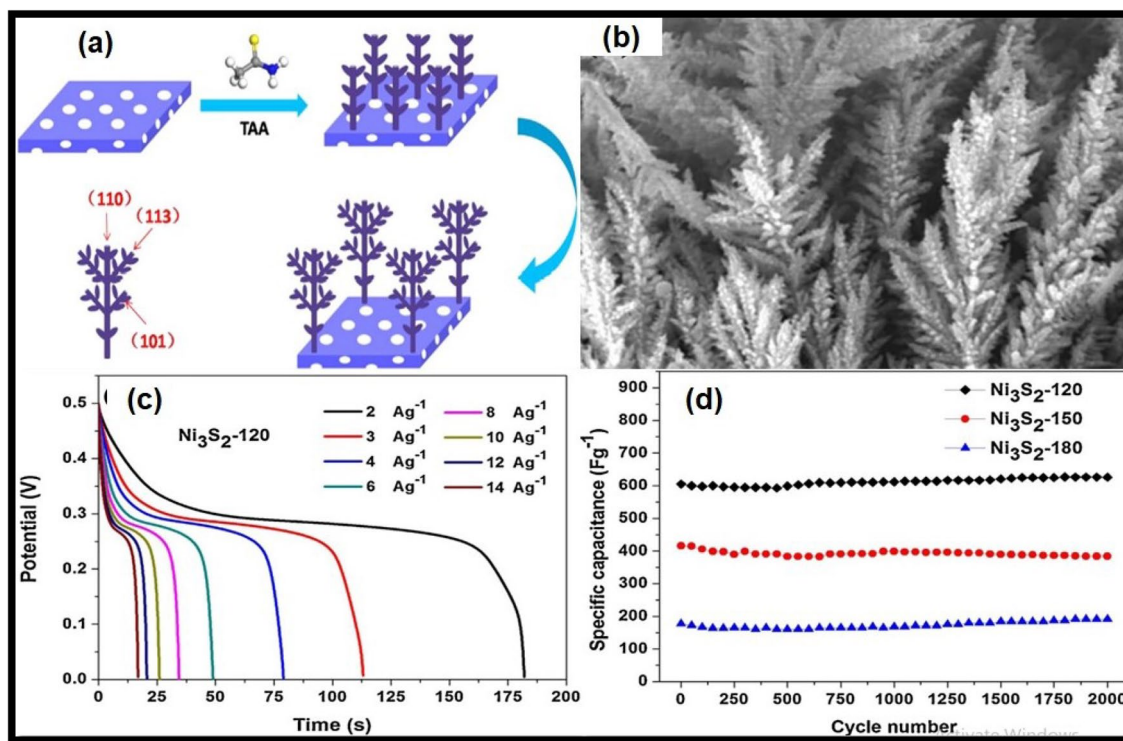


Figure 4: (a) Schematic illustration of synthesis process, (b) SEM image of the Ni_3S_2 3D hierarchical dendrites obtained at 120°C for 6 h (c) GCD curves for Ni_3S_2 hierarchical dendrites at different current densities (2, 4, 6, 8, 10, 12, 14Ag^{-1}), and (d) cycle life of Ni_3S_2 prepared at different temperatures. (Reprinted with permission from ref. [89]).

was a promising electrode material which exhibits excellent supercapacitor behavior [108].

Transition metal diselenides (TMDSe)

Transition metal diselenides exhibits characteristics comparable to transition metal sulfides as selenium is located in the same group as sulfur. The volume energy density and rate capability of transition metal diselenides as cathode materials might be higher than those of transition metal sulfides because of relatively higher density and electrical conductivity of selenium. Recently, transition metal diselenides (NiSe_2 , CoSe_2 and MnSe_2) were found to be promising materials for application to electrochemical energy storage devices. In transition metal diselenides, a sandwich structure is always observed with the metal atom at the center of two selenide layers. The atoms in these three layers are covalently linked via weak Vander Waal forces between the individual sheets. The later force is weak enough for other atoms to easily and reversibly intercalate into the interchain space and form an intercalation compounds or intercalates, enabling energy to be stored in the layered conductors [109, 110].

Nickel and selenium can be combined to make a variety of nickel diselenides including nonstoichiometric compounds with composition, microstructure, and morphologies, affecting the compounds properties. Penroseite nickel diselenide (NiSe_2)

is a Pauli magnetic metal with a pyrite-type cubic structure and a resistivity below $10^{-3}\ \Omega\ \text{cm}$, making it a promising electrode material for supercapacitors. Arul et al. successfully synthesized hexapod-like 2D transition metal dichalcogenide (TMD) NiSe_2 structures via hydrothermal method and studied its electrochemical properties as a supercapacitor for the first time. It was observed that the structural and compositional results confirmed the presence of orthorhombic phase of NiSe_2 in the synthesized hexapod-like NiSe_2 structures. The electrochemical studies revealed that the fabricated hexapod-like NiSe_2 exhibited specific capacitance of $75\ \text{Fg}^{-1}$ and retained 94% of its initial capacitance at a current density of $1\ \text{mA}\ \text{cm}^{-2}$ even after 5000 charge/discharge cycles [111]. Gu et al. successfully fabricated NiSe_2 nanoarrays with white beech mushroom-like structure via hydrothermal method. The as-prepared NiSe_2 nanoarrays belong to the cubic phase having stem diameter ranging 50-70 nm, length about 500 nm and the diameter of the umbrella cover about 50 nm. The obtained unique mushroom-like structure possesses large surface area and enhanced the electrochemical active sites. The controlled experiment revealed that this mushroom-like NiSe_2 nanoarrays exhibited high specific capacitance of $262\ \text{mAhg}^{-1}$ with cyclic stability of 83.4% even after 8,000 cycles. Subsequently, mushroom-like NiSe_2 nanoarrays and activated carbon were further assembled as hybrid supercapacitors. They used mushroom-like NiSe_2 nanoarrays as

positive electrode and activate carbon as negative electrode to make hybrid supercapacitors, exhibiting an energy density of 33 Whkg⁻¹ with 90.3% retention of its initial capacitance. They also reported that the mushroom-like NiSe₂ nanoarrays not only a promising electrode materials but also provides a new candidate for the field of flexible, smart and portable devices [112]. Pazhamalai et al. successfully fabricated 2H-MoSe₂ nanosheets via hydrothermal method. The cyclic voltammetric studies revealed that MoSe₂ symmetric supercapacitor delivered a specific capacitance of 25.13 Fg⁻¹ at scan rate of 5mVs⁻¹ and charge/discharge results revealed that the MoSe₂ symmetric supercapacitor have specific capacitance of 16.25 Fg⁻¹ at current density of 0.75 Ag⁻¹ with power density of 7.5 kWkg⁻¹ at 5 Ag⁻¹ and 87% specific capacitance retention after 10,000 cycles. They further reported that nanosheet-like structure were the main reason behind this improvement in electrochemical performance because MoSe₂ exhibited high surface area with a wide range of pore size which facilitated more active sites for intercalation [113].

Gu et al. successfully synthesized N-doped reduced graphene oxide/NiSe₂ composites via simple two-step process which contains hydrothermal preparation of Ni(OH)₂ precursor and then solvothermal synthesis of N-rGO/NiSe₂ composites with different amount of rGO (reduced graphene oxide). They reported that the as-synthesized N-rGO act as a supporter of NiSe₂ nanoparticles to prevent them from aggregation which leads to the increase in specific surface area and electrical conductivity of material. It was reported that N-rGO/NiSe₂ composite electrodes delivered high specific capacitance of 2451.4 Fg⁻¹ at a current density of 1 Ag⁻¹ using 3 M KOH as electrolyte. The maximum energy density of N-rGO/NiSe₂ composite electrodes were reported as 40.5 Whkg⁻¹ at a power density of 841.5 Wkg⁻¹, with 85.1% retention of its initial capacitance after 10,000 cycles at 5Ag⁻¹. The higher specific capacitance and cyclic stability was due to enhancement of surface area and conductivity of electrode materials [114]. Gopalkrishnan et al. successfully fabricated unique binder-free polyaniline (PANI) sheathed 3D crumpled CoSe₂ nanoparticles on Ni-foam (PANI/CoSe₂/NF) electrode via simple electrodeposition method. The PANI/CoSe₂/NF electrode exhibited excellent electrochemical performance in supercapacitor applications due to its high surface area, synergistic effects between CoSe₂ nanostructures and PANI sheets, high electrical conductivity, and hydrophilic functional groups of PANI, which contribute to lower internal resistance and effective diffusion of ions. It was observed that the PANI/CoSe₂/NF as supercapacitor electrode delivered high specific capacitance of 1980 Fg⁻¹ or 3825 Fg⁻¹ and a specific capacity of 792 Cg⁻¹ at 2 Ag⁻¹ in a three-electrode cell arrangement [115].

Miao et al. successfully synthesized CoSe₂/rGO nanocomposites via low-cost microwave method [Fig. 5(a)], they investigated the impact of rGO content on crystalline structure, microstructure [Fig. 5(b), (c)], and energy storage devices

performance. It was observed that the CoSe₂/rGO sample with 35.2% rGO exhibited excellent specific capacitance of 761 Fg⁻¹ as well as extraordinary durability with 8% capacity drops even after 10,000 cycles as displayed in [Fig. 5(d)–(f)]. It was noticed that all solid-state hybrid supercapacitor CoSe₂/rGO/active carbon were used to expand the voltage window, resulting in a higher energy density of 43.1 Whkg⁻¹ as the hybrid device presented a remarkable durability of 90% retention even after 10,000 cycles [116]. Metal organic framework (MOF) derived CoSe₂ nanoparticles embedded into an N-doped carbon nanosheets (CoSe₂/NC) were successfully synthesized via one-step derivation and selenylation, as selenylation was an effective method to enhance the electrochemical properties of electrode materials. The obtained triangular nanosheets facilitated the full contact of electroactive materials and the electrolyte, improving the productivity of electrode material and CoSe₂/NC composite provided excellent electronic conductivity. It was observed that the CoSe₂/NC composite were directly grown on Ni-foam as nanosheets rather than on other materials as powders, the results revealed that the CoSe₂/NC sample exhibited high specific capacity of 120.2 mA hg⁻¹ at 1 Ag⁻¹, with good cyclic ability of 92% even after 10,000 cycles. Furthermore, an asymmetric supercapacitor CoSe₂/NC-400/AC exhibited maximum energy density of 40.9 Whkg⁻¹ at 980 Wkg⁻¹. These findings revealed that the as-synthesized CoSe₂/NC-400/AC electrodes acquired potential for use in supercapacitor applications [117]. Gopi et al. successfully fabricated WSe₂/rGO composite via one-step hydrothermal method in which WSe₂ nanosheets were implanted with the rGO sheets. The obtained sample possess mesoporous structure with large surface area which was beneficial for better electrochemical performances. It was found that the WSe₂/rGO-based supercapacitor electrode exhibited maximum specific capacitance of 389 Fg⁻¹ at 1 Ag⁻¹, a maximum energy density of 34.5 Whkg⁻¹ and a maximum power density of 400 Wkg⁻¹ as well as long cycling stability of 98.7% after 3000 cycles at 7 A g⁻¹ [118]. Marri et al. successfully fabricated VSe₂/rGO hybrids of highest quality at different concentrations of graphene oxide via one-step hydrothermal method. It was observed that the supercapacitor performance was enhanced in the case of the hybrid obtained at 0.3% of graphene oxide due to synergistic effect. They reported that the resulting VSe₂/rGO sample exhibited high specific capacitance of 680 Fg⁻¹ at 1 Ag⁻¹ which was found to be ~6 and ~5 times higher than bare VSe₂ and bare rGO, respectively, high energy density of 212 Whkg⁻¹, power density of 3.3 kWkg⁻¹ and retained 81% of initial capacitance even after 10,000 cycles [119].

Transition metal phosphides (TMP)

Recently, transition metal phosphides (TMPs) were found to be promising materials for various applications such as electrocatalysis, lithium-ion batteries, supercapacitors, and photocatalysis

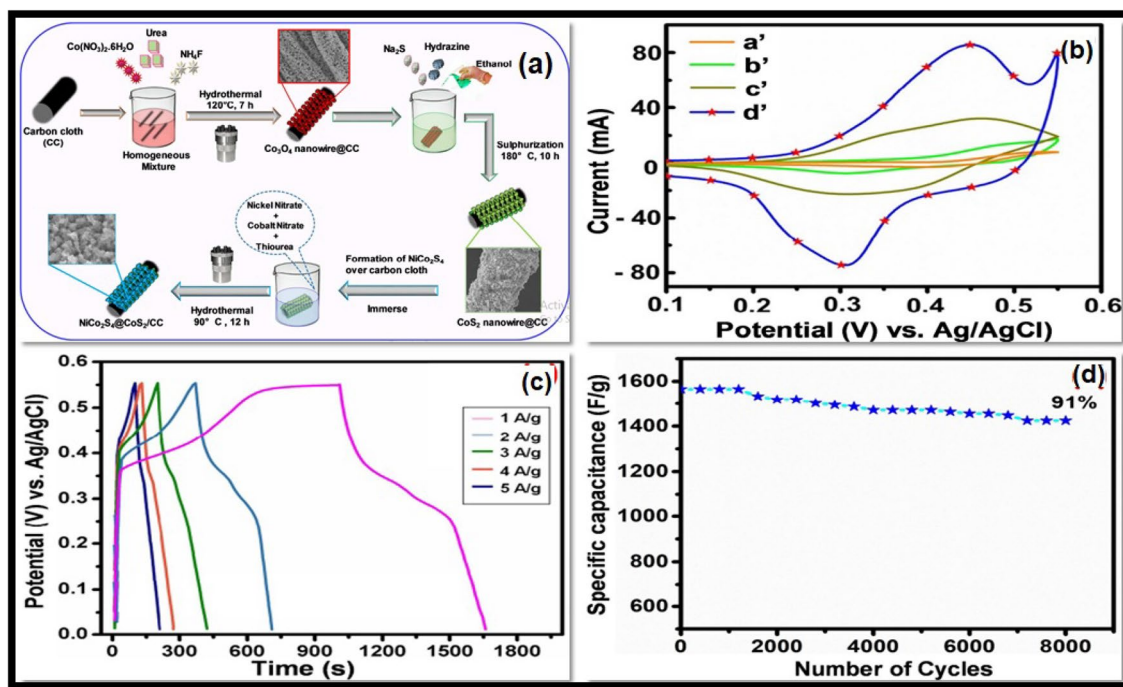


Figure 5: (a) Schematic of the fabrication procedure to synthesis the flexible hybrid NiCo₂S₄@CoS₂ nanostructures on carbon cloth (CC), (b) (a) CV curves of (a') CC, (b') Co₃O₄@CC, (c') CoS₂@CC, and NiCo₂S₄@CoS₂@CC (d') hybrid electrodes at a 5 mVs⁻¹ scan rate in 2 M KOH., (c) GCD curves of the NiCo₂S₄@CoS₂@CC hybrid electrode at various current 10 densities (1 to 5 Ag⁻¹) (d) specific capacitance retention of the NiCo₂S₄@CoS₂@CC 4 hybrid electrode at current density of 1 Ag⁻¹. (Reprinted with permission from ref. [102]).

[120]. Compared to the transition metal oxides/hydroxides and conducting polymers, transition metal phosphides have excellent electrical conductivity which led to fast electron transport, resulting to provide high power density in supercapacitor applications [121]. The electrochemical performance of the transition metal phosphides as electrode materials for supercapacitor application depends upon surface structures, chemical composition and the metal to phosphorus ratio [122].

Recently, researchers explored various transition metal phosphides for their electrochemical performance. The Copper (I) phosphide (Cu₃P) nanostructure with tube-like morphology has been directly synthesized on copper foil via two-step process of electro-oxidation and phosphidation. The Cu₃P electrodes were used as a negative electrode for supercapacitor applications and showed specific capacitance of 300.9 Fg⁻¹ with energy density of 44.6 Whkg⁻¹ and power density of 17,045.7 Wkg⁻¹. They also reported that electrodes were found to be stable after 5000 cycles with 81.9% of their initial capacitance at current density of 10 mAcm⁻² [123].

The cheap transition metal (e.g., Nickel, Cobalt or Iron) phosphides owing to their metalloidal characteristics and superior electrical conductivity have emerged as appreciable substitute for transition metal oxides and hydroxides which are kinetically unfavorable for fast electron transport required for high power density in supercapacitors [124].

Liang and co-workers have synthesized Cobalt phosphide (Co₂P) nanoshuttles via microwave-assisted hydrothermal treatment using cobalt chloride and yellow phosphorus as precursors. The synthesized Co₂P showed excellent electrochemical behavior with high specific capacity of 246 Fg⁻¹ at 1 Ag⁻¹ and high retention capacity of 72% after 1000 cycles. They have reported that the novel one-dimensional nanostructure of Co₂P provided a larger ion accessible area and effectively avoided agglomeration among active particles resulting in better electrochemical performance [124]. It was reported that CoP can be used as a promising material for negative electrode material for high-performance supercapacitor applications. The three-dimensional cobalt phosphide (CoP) nanowire arrays have been synthesized on carbon cloth by a hydrothermal method, followed by low-temperature phosphidation. These CoP nanowire arrays were used as a negative electrode and MnO₂ nanowire arrays were used as positive electrode in an asymmetric supercapacitor, which showed high specific capacitance of 571.3 mFcm⁻² at a current density of 1 mAcm⁻². The energy density of 0.69 mWhcm⁻³ was obtained at power density of 114.2 mWcm⁻³ with 82% of initial capacitance after 5000 charge/discharge cycles. This outstanding electrochemical performance of the CoP nanowire arrays was stated to be because of three main aspects, “first, the superior electrical conductivity of CoP facilitated electron transfer within the

electrode. Second, the 3D configuration of the CoP nanowire arrays offered a large surface area as well as the short ionic and electronic paths. Last, the direct growth of the CoP nanowire arrays on carbon cloth provided robust mechanical adhesion and good electrical contact” [125]. The Mn-doped cobalt cluster arrays on Ni-foam (Mn-CoP/NF) have been successfully fabricated via hydrothermal process with a fine morphology. The asymmetric supercapacitor was fabricated using Mn-CoP/NF electrodes as anode and activated carbon as cathode. It was reported that the fabricated supercapacitor showed specific capacitance of 8.66 F cm^{-2} at 1 mAcm^{-2} with high energy densities of 35.21 Whkg^{-1} and 30.87 Whkg^{-1} at power densities of 193 Wkg^{-1} and 1939 Wkg^{-1} , respectively, and this appreciable electrochemical performance can be attributed to lower diffusion resistance of Mn-CoP/NF electrode material [126].

The 3D porous Ni_2P nanoarrays have been synthesized on a Ni-foam ($\text{Ni}_2\text{P}/\text{NF}$) using the hydrothermal process. Afterward, nanocarbon has been embedded on $\text{Ni}_2\text{P}@\text{NF}$ ($\text{Ni}_2\text{P}-\text{C}/\text{NF}$) by ethylene gas using a dielectric discharge. The $\text{Ni}_2\text{P}-\text{C}/\text{NF}$ were employed as the positive electrode, while porous activated carbon acted as the negative electrode in the hybrid supercapacitor which provided a high areal and gravimetric capacitance of $318.8 \mu\text{Ahcm}^{-2}$ and 106.2 mAhg^{-1} , respectively, at 1 Ag^{-1} . The positive synergistic effect and nanoflake structure, which had provided more active surface sites were responsible for high electrochemical performance of $\text{Ni}_2\text{P}-\text{C}/\text{NF}$ [127]. 1D interconnected porous nickel cobalt phosphide nanowires have been synthesized via hydrothermal method and subsequent phosphorization treatment. The obtained bimetallic phosphides exhibit higher specific capacitance of 1395 F g^{-1} than the monometallic nickel phosphide (920 Fg^{-1}) and cobalt phosphide (568 Fg^{-1}) at 1 Ag^{-1} , with an energy density of 53.31 Whkg^{-1} and a power density of 46.53 kWkg^{-1} along with the capacitance retention of 83.04% after 20,000 cycles. It was reported that the as-prepared NCP nanowire has displayed better performance owing to the rich exposed redox active sites and fast charge transport pathway [128].

The bimetallic phosphides stimulate manifold valence states for more redox reactions and hence show higher specific capacities and catalytic activities than monometallic phosphides. Shou et al. synthesized self-assembled three-dimensional Ni-Fe-P nanosheet array on the Ni-foam via hydrothermal method followed by phosphidation. It was reported that Ni-Fe-P/Ni electrode showed excellent specific capacitance of 1358 C g^{-1} at 5 mA cm^{-2} with an outstanding energy density of 50.2 Whkg^{-1} at the power density of 800 Wkg^{-1} . The electrodes were found to maintain 91.5% initial specific capacitance after 10,000 cycles. It was reported that this remarkable performance is ascribed to the porous structure, the increased specific surface area, active sites and binder-free construction of Ni-Fe-P electrodes [129]. The zinc nickel phosphide nanosheet (Zn-Ni-P) arrays has been

fabricated by adopting a simple and cost-effective hydrothermal and subsequent effective phosphorization technique and showed specific capacitance of 384 mAh g^{-1} at a current density of 2 mA cm^{-2} . Moreover, Zn-Ni-P electrodes showed excellent energy density of 90.12 Whkg^{-1} at a power density of 611 Wkg^{-1} and extraordinary cycling stability of 93.05% of initial capacity after 20,000 cycles at a current density of 15 mAcm^{-2} . It was further reported that these outstanding electrochemical performances were attributed to the 3D hierarchical nanostructures, porous nanonetworks, improved conductivity, and synergistic interaction between the active components of Zn-Ni-P nanosheet arrays [130].

Though the single and binary metallic phosphides emerged as impressive electrode materials, the ternary metallic phosphides perform better than their single and binary counterparts. The 3D flower-like ternary metallic manganese-nickel-cobalt phosphides (MNCs) with different metal proportions have been prepared using electrodeposition followed by low-temperature PH 3 plasma treatment with various morphologies. The MNCP electrodes showed an ultra-high capacity of 1690 C g^{-1} in the three-electrode system. The authors reported that besides the positive synergistic effect of combining the three transition metals, the outstanding performance is ascribed to the intriguing architecture with 3D networks and porous nanosheets which enhances the capacity performance by facilitating fast electrolyte transport and active sites and hence demonstrated MNCP as a suitable SC electrode material [131].

Ternary transition metal ferrites

Iron-based materials are being used for a wide range of applications such as medical [132], memory devices [133], energy storage devices [134], sensing devices [135], catalyst [136], biomedical [137], and magnetic resonance imaging [138]. Iron is the fourth most abundant elements on the earth, non-toxic, and cost-effective compared to other transition metals. The ferrites are significant magnetic materials classified as spinel with general formula MFe_2O_4 ($\text{M} = \text{Mn, Fe, Co, Ni, Co, Zn, etc.}$) or a garnet represented as $\text{M}_3\text{Fe}_5\text{O}_{12}$ ($\text{M} = \text{rare-earth cations}$) or a hexaferrite ($\text{SrFe}_{12}\text{O}_{19}$ and $\text{BaFe}_{12}\text{O}_{19}$) or an orthoferrite with general formula MFeO_3 ($\text{M} = \text{rare-earth cations}$) on the basis of their magnetic properties and crystal structures. Among these groups, the ternary transition metal ferrites or spinel ferrites (MFe_2O_4) with M^{2+} and Fe^{3+} occupying the tetrahedral and octahedral sites are captivating because of their impressive magnetic, electrical, and optical properties as well as their ability to exhibit different redox states and electrochemical stability [139, 140]. These materials are found to be suitable for energy storage devices [141], electrochemical applications [142], environmental applications [143], and biological applications [144].

The ternary transition metal ferrites may also consist of a mixture of two divalent metal ions, in which the ratio of these divalent ions may vary, and they are referred to as mixed ternary transition metal ferrites. In the challenging field of supercapacitors, the reports on these mixed ternary transition metal ferrites with general formula $A_xB_{1-x}Fe_2O_4$ are really fascinating [140].

These ternary transition metal ferrites show remarkable electrochemical properties, owing to the multiple oxidation states of the metal ions which make them suitable for electrode materials in supercapacitor application. The multiple valences of the metal cations and their complex chemical composition enhance the electrochemical behavior of supercapacitors [145].

Ferrite nanostructures with tunable sizes and morphologies including nanocrystals [146], hollow spheres [147], nanorods/nanowires [148], and nanotubes [149] have been successfully synthesized using various synthetic techniques, such as hydrothermal/solvothermal [150], thermolysis [151], template-based [152], sol-gel [153], co-precipitation [154], and electrochemical synthesis [155].

The $MnFe_2O_4$ nanoparticles have been successfully synthesized via co-precipitation method. The synthesized particles were reported to be spherical in shape with diameter between 20 and 50 nm. It was further reported that $MnFe_2O_4$ nanoparticles electrodes showed a maximum specific capacitance of 430 Fg^{-1} using 1 M Li_3PO_4 electrolyte [156]. The $ZnFe_2O_4$ nanoparticles were synthesized using a weak ultrasonic irradiation technique. The specific capacitance of these nanoparticle electrodes was 712 Fg^{-1} at scan rate of 2 mVs^{-1} , with 96.6% retention after 2000 cycles [157].

It was reported that the morphology of the nanoparticles depends upon the molarity of the precipitating agent. The monodispersed $CuFe_2O_4$ nanoparticles have been synthesized via solvothermal method at various molarity of the precipitating agent KOH. It was found that the size of spherical monodispersed $CuFe_2O_4$ nanoparticles reduces upon increasing the molarity of KOH. Further, the maximum specific capacitance was found for the electrodes prepared using $CuFe_2O_4$ nanoparticles synthesized at 10 M KOH which was 189.2 F/g at current density of 0.5 Ag^{-1} with 84% initial capacitance retention after 1000 cycles [158].

Kennaz and co-workers have synthesized $CoFe_2O_4$ nanoparticles by co-precipitation method and hydrothermal method, using various precursor such as nitrates, chlorides, and acetates. It was reported that the optimized condition for the co-precipitation method was for using nitrate-based precursors under $80 \text{ }^\circ\text{C}$ reaction temperature and there was no noticeable difference observed in hydrothermally prepared samples. The size of single-phase nanoplatelet-shaped $CoFe_2O_4$ particles were between 11 and 26 nm. They further reported that hydrothermally prepared samples showed specific capacitance of 429 F/g at a current density of 0.5 Ag^{-1} , with excellent capacitance retention of 98.8% after 6000 cycles at 10 Ag^{-1} [159].

It was reported that the cyclic stability and rate performances can be improved by the doping of rare-earth (RE) elements. For the first time, Ghulam et al. synthesized cerium-doped cobalt spinel ferrite ($Ce_xCo_2Fe_{2-x}O_4$ ($x=0, 0.3, 0.5$)) nanoparticles via hydrothermal method for supercapacitor application as illustrated in Fig. 6(a). They reported that Ce doping has a strong effect on the structural, optical, and electrochemical properties of the cobalt ferrite nanostructure. They found that $Ce_{0.3}CoFe_{1.7}O_4$ has particle size range from 40 to 220 nm with maximum number of particles lying in the range of 120–140 nm, whereas $Ce_{0.5}CoFe_{1.5}O_4$ has particle size range is from 40–180 nm with the maximum number of particles laying in the range of 80–100 nm [Fig. 6(b)]. They concluded that reduction of particle size upon increasing the Ce concentration was because Ce replace Fe at octahedral site of the cubic crystal of $Ce_xCo_2Fe_{2-x}O_4$. Further, the highest specific capacitance of 937.50 Fg^{-1} was obtained for $Ce_{0.5}Co_2Fe_{1.5}O_4$ at a current density of 0.5 Ag^{-1} [Fig. 6(c)] with 82.3% of initial capacitance retention after 4000 cycles. They also reported that the high specific capacitance of the doped samples was because of the two main reasons, “first, CeO goes on the interstitial sites of the cobalt ferrite lattice and enhances the chemical activities of the electrode material and secondly the ionic radii of Fe^{3+} and Ce^{3+} are 69 pm and 115 pm, respectively, and due to its higher ionic radius, Ce^{3+} forms the local distortion in the crystal lattice of $CoFe_2O_4$, the diffusion rate of protons increases because exchange reaction and electron can escape from $CoFe_2O_4$ more easily”. Figure 6(d) represents the graph between specific capacitance and scan rate [160].

Sethi and co-workers have synthesized $NiFe_2O_4$ nanoparticles via solvothermal method. It was reported that the spherical nanoparticles were uniformly distributed and of the size ranging from 13–17 nm. They reported that electrochemical performance has revealed the specific capacitance to be 368 Fg^{-1} at a current density of 1 Ag^{-1} with energy density of 10.4 Whkg^{-1} and power density of 225.8 Wkg^{-1} at the current density of 1 Ag^{-1} . They also reported that the superior electrochemical performance of the nanoparticles is mainly ascribed to the nanoscale morphology with high surface area and high porosity providing substantial electroactive sites for the electrolyte ions insertion/de-insertion apart from sustaining its mechanical stability during the electrochemical process [161]. It was reported that nanocrystallites of pure and mixed ternary ferrites such as $NiFe_2O_4$, $CuFe_2O_4$, $CoFe_2O_4$, $Ni_{0.5}Cu_{0.5}Fe_2O_4$, $Ni_{0.5}Co_{0.5}Fe_2O_4$, and $Cu_{0.5}Co_{0.5}Fe_2O_4$ can be synthesized via self-combustion method. The as-synthesized samples were reported to exhibit a pure spinel crystal structure with the crystallite sizes ranged from 12–47 nm. The capacitance values for these ferrites were reported in the order as $CuCoF > NiCoF > CoF > NiCuF > CuF > NiF$, with the highest specific capacitance of 220 F/g for $Cu_{0.5}Co_{0.5}Fe_2O_4$, with an energy density of 34.7 Whkg^{-1} and power density of 605 Wkg^{-1} [162].

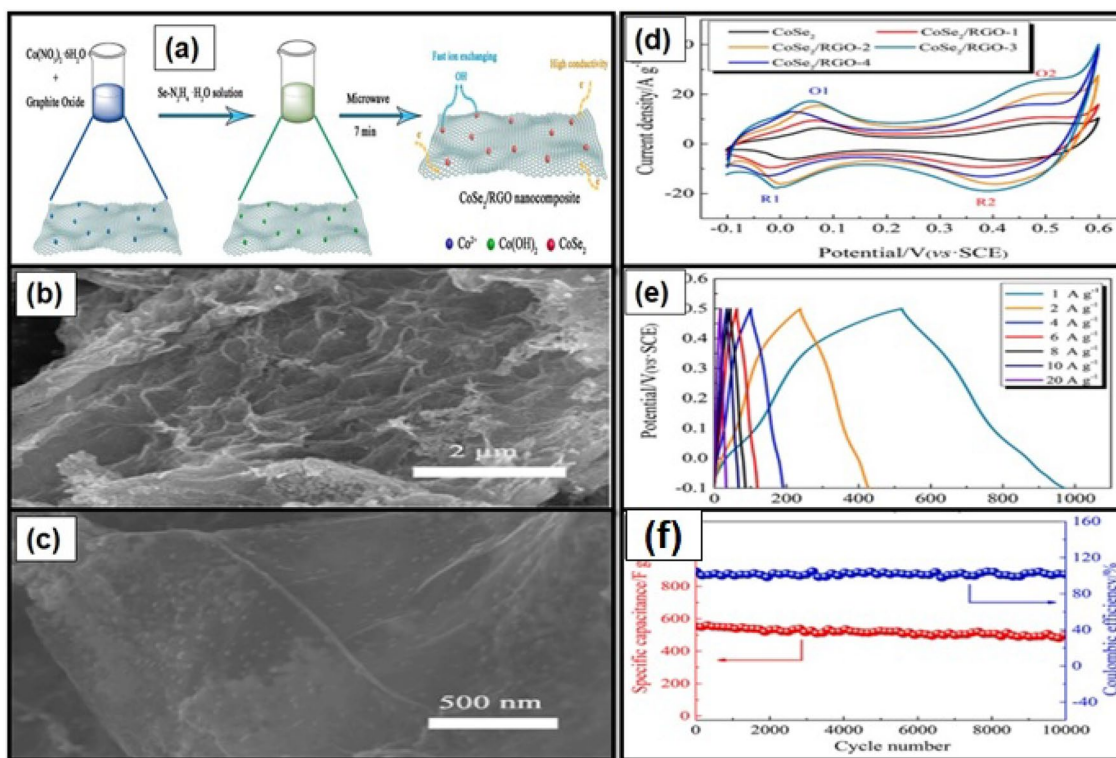


Figure 6: (a) Schematic diagram of fabrication process for CoSe₂/rGO composites, (b) & (c) SEM images of CoSe₂/RGO-3 at different magnifications (d) CV curves of CoSe₂/RGO-3 (e) GCD curve, (f) Durability test. (Reprinted with permission from ref. [116]).

In order to find a suitable material for supercapacitor applications, the Ni_{0.5}Zn_{0.5}Fe₂O₄ nanomaterial were synthesized as active materials (NZF) and directly on to Ni-foam (NZF@NF) via hydrothermal techniques. The synthesized materials were reported to have thin hexagonal platelets like morphology with the particle size ranging between 27–49 nm. The NZF and NZF@NF electrode delivered a high specific capacity of 151.1 Fg⁻¹ and 504 Fg⁻¹, respectively, at a current density of 1 Ag⁻¹. This superior performance was ascribed to the increase in electroactive area due to the mesh structure of the nickel foam and the higher capacity of NZF@NF can be attributed to the higher electrical conductivity and porous structure of the nickel foam that facilitate the diffusion of ions and electrons [163] (Fig. 7).

Conclusions, challenges, and future perspectives

In summary, this review insights into the recent developments, challenges and future perspectives of various transition metal-based nanomaterials including oxides, sulfides, selenides, nitrides, ferrites, phosphides, and their derivatives for their application in supercapacitors. Transition metal-based nanomaterials owing to their unique properties and architectures led great development in the field of electrochemical

energy storage. The advantages of transition metals such as exclusive d-electron configurations, cost-effectiveness, synergistic effect of multi-metal atoms, outstanding stability are mainly advantageous for the electrochemical supercapacitors. Various morphologies including nanorod, nanotubes, nanoflowers and nanospheres are pre-requisite to obtaining good electrochemical properties. These specific nanostructures deliver large surface area and minimize the diffusion paths of electrolyte ions and electrons, resulting into plenty of free spaces for buffering the large volume change of active materials throughout the charge/discharge processes. Moreover, insertion of additional elements provides more redox reaction active sites in the electrode materials. Over recent years research is going on the transition metal oxides, and they have great advantages in terms of abundant resource and cost-effectiveness. Also, their higher specific capacitance in comparison to carbon-based materials and conductive polymers as well as relatively mature production technology enable them frequently used candidate in the commercial field. However, relatively low electrical conductivity restricts their large-scale commercial applications by limiting high charge/discharge kinetics of the electrode material. To overcome this issue, lots of effort are focused on synthesis of nanostructured electrode material having large surface area and their heterostructures/composites with synergistic effect. Transition metal sulfides,

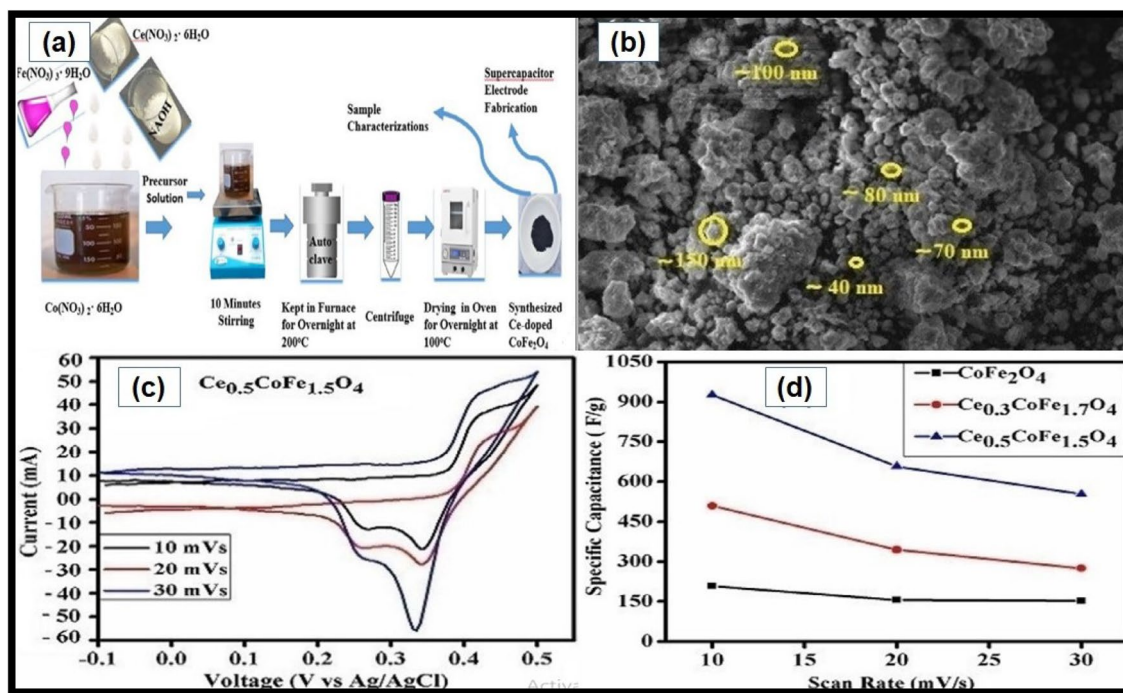


Figure 7: (a) Schematic of synthesis process of pure and Ce-doped CoFe_2O_4 , (b) SEM image of $\text{Ce}_x\text{CoFe}_{x-2}\text{O}_4$ ($x=0.5$), (c) CV curves of $\text{Ce}_x\text{CoFe}_{x-2}\text{O}_4$ ($x=0.5$) and (d) Plot between specific capacitance and scan rate. (Reprinted with permission from Ref. [160]).

selenides are also considered potential electrode material due to their intrinsic enhanced electrical conductivity and electrochemical activity. Sulfur has lesser electronegativity than that of oxygen which facilitates easy electron transfer in the metal sulfide structure than that in the metal oxide. However, their capacitance and energy density still need to be improved; therefore synthesis process and effective control of structure along with production cost needs further exploration. Moreover, transition metal nitrides are also promising active electrode material for supercapacitor application due to their low cost, environment friendly nature and higher volumetric energy densities. Nitride formation also undergo some issues due to thermodynamic barrier that includes the formation and deformation of triple bond between nitrogen atoms. Hybrid heterostructures of these materials with carbonaceous compounds led improvement in the specific capacitance and energy density of the transition metal nitride-based supercapacitors. The abundance of oxygen vacancies and remarkable conductivity enables transition metal ferrites to hold extraordinary energy densities. Volume fluctuations through charge and discharge process and low cycling stability are some issues which need to be focused on transition metal ferrites. Designing ferrites with large surface areas, huge porosity, making composites with carbonaceous materials and conducting polymers that reduce the irreversible capacity loss are essential to overcome these issues. Various studies on both simple and complex transition metal phosphides suggests them desirable

candidate for electrodes material in hybrid supercapacitors in comparison with their corresponding oxides, sulfides, and selenides counterpart. The major bottleneck of this category material is their sluggish reaction kinetics and volumetric expansion during charge discharge process, resulting into deterring the rate capability and cycling stability of transition metal phosphide-based supercapacitors. Doping and designing composites are some of the approaches that can be used for the enhanced electrochemical performance. Some insights in future perspectives are highlighted in order to achieve high electrochemical performance of transition metal-based nanomaterials.

- (1) Optimization of the design and fabrication of these nanomaterials for specifically, supercapacitor application by systematic theoretical and experimental investigations are necessary.
- (2) Selection of dopant, making composites/heterojunctions, core shell structures for further improvement in the performance of transition metal-based nanomaterials. We may emphasize on making nanocomposites using various novel materials such as carbonaceous materials, oxides and conducting polymers that offers more active sites for particular application.
- (3) The structure and morphological control along with different strategies such as tailoring and engineering for in-depth understanding are essential for practical implementation of electrochemical devices.

- (4) Synthesis of electroactive nanomaterials having high conductivity and porous structure that provide a large specific area, shorter diffusion length for electrolyte ions with low cost and environment friendly production.
- (5) It is also important to significantly improve the research for the flexible, lightweight, high energy supercapacitors, to practically fulfill the demand of consumer.
- (6) It is also necessary to focus on simplifying the synthesis methods and strategies for large-scale and low-cost production.

Now a days, researchers have attained very high values of energy and power densities for transition metal-based supercapacitors by utilizing various creative approaches. However, further improvements and inventions are still required to meet out the current energy demand of the society. Therefore, the progress in the transition metal-based nanomaterials paves a way for bright and exciting future and further reform the future of energy storage industry.

Author contribution

All authors have equal contribution.

Declarations

Conflict of interest The authors declare no conflicts of interest.

Data availability

The data/findings reported in this review article is available in respective references and doi is given for all references in this article.

References

1. G. Wang, L. Zhang, J. Zhang, A review of electrode materials for electrochemical supercapacitors. *Chem. Soc. Rev.* **41**(2), 797–828 (2012). <https://doi.org/10.1039/C1CS15060J>
2. X. Wang, G. Pawar, Y. Li, X. Ren, M. Zhang, B. Lu, A. Banerjee, P. Liu, E.J. Dufek, J.-G. Zhang, Glassy Li metal anode for high-performance rechargeable Li batteries. *Nat. Mater.* **19**(12), 1339–1345 (2020). <https://doi.org/10.1038/s41563-020-0729-1>
3. Y. Liu, X. Li, W. Shen, Y. Dai, W. Kou, W. Zheng, X. Jiang, G. He, Multishelled transition metal-based microspheres: synthesis and applications for batteries and supercapacitors. *Small* **15**(32), 1804737 (2019). <https://doi.org/10.1002/sml.201804737>
4. M.D. Hager, B. Esser, X. Feng, W. Schuhmann, P. Theato, U.S. Schubert, Polymer-based batteries—flexible and thin energy storage systems. *Adv. Mater.* **32**(39), 2000587 (2020). <https://doi.org/10.1002/adma.202000587>
5. H. Jin, S. Dai, K. Xie, Y. Luo, K. Liu, Z. Zhu, L. Huang, L. Huang, J. Zhou, Regulating interfacial desolvation and deposition kinetics enables durable Zn anodes with ultrahigh utilization of 80%. *Small* **18**(4), 2106441 (2022). <https://doi.org/10.1002/sml.202106441>
6. Y. Zhou, C.H. Wang, W. Lu, L. Dai, Fiber-shaped energy-storage devices: recent advances in fiber-shaped supercapacitors and lithium-ion batteries. *Adv. Mater.* **32**(5), 2070037 (2020). <https://doi.org/10.1002/adma.202070037>
7. S. Zheng, X. Shi, P. Das, Z.S. Wu, X. Bao, Microscale energy-storage devices: the road towards planar microbatteries and micro-supercapacitors: from 2D to 3D device geometries. *Adv. Mater.* **31**(50), 1970351 (2019). <https://doi.org/10.1002/adma.201970351>
8. F. Béguin, V. Presser, A. Balducci, E. Frackowiak, Carbons and electrolytes for advanced supercapacitors. *Adv. Mater.* **26**(14), 2219–2251 (2014). <https://doi.org/10.1002/adma.201304137>
9. F. Wu, H. Yang, Y. Bai, C. Wu, Paving the path toward reliable cathode materials for aluminum-ion batteries. *Adv. Mater.* **31**(16), 1806510 (2019). <https://doi.org/10.1002/adma.201806510>
10. A. Konarov, N. Voronina, J.H. Jo, Z. Bakenov, Y.-K. Sun, S.-T. Myung, Present and future perspective on electrode materials for rechargeable zinc-ion batteries. *ACS Energy Lett.* **3**(10), 2620–2640 (2018). <https://doi.org/10.1021/acsenerylett.8b01552>
11. S. Yang, S. Wang, X. Liu, L. Li, Biomass derived interconnected hierarchical micro-meso-macro-porous carbon with ultrahigh capacitance for supercapacitors. *Carbon* **147**, 540–549 (2019). <https://doi.org/10.1016/j.carbon.2019.03.023>
12. Y. Zhang, S. Yang, S. Wang, X. Liu, L. Li, Microwave/freeze casting assisted fabrication of carbon frameworks derived from embedded upholder in tremella for superior performance supercapacitors. *Energy Storage Materials* **18**, 447–455 (2019). <https://doi.org/10.1016/j.ensm.2018.08.006>
13. R. Dubey, V. Guruviah, Review of carbon-based electrode materials for supercapacitor energy storage. *Ionics* **25**(4), 1419–1445 (2019). <https://doi.org/10.1007/s11581-019-02874-0>
14. L. Wang, L. Wen, Y. Tong, S. Wang, X. Hou, X. An, S.X. Dou, J. Liang, Photo-rechargeable batteries and supercapacitors: Critical roles of carbon-based functional materials. *Carbon Energy* **3**(2), 225–252 (2021). <https://doi.org/10.1002/cey2.105>
15. A. Riaz, M.R. Sarker, M.H.M. Saad, R. Mohamed, Review on comparison of different energy storage technologies used in micro-energy harvesting, WSNs, low-cost microelectronic devices: challenges and recommendations. *Sensors (Basel)* (2021). <https://doi.org/10.3390/s21155041>
16. A. Borenstein, O. Hanna, R. Attias, S. Luski, T. Brousse, D. Aurbach, Carbon-based composite materials for supercapacitor

- electrodes: a review. *J. Mater. Chem. A* **5**(25), 12653–12672 (2017). <https://doi.org/10.1039/C7TA00863E>
17. A. González, E. Goikolea, J.A. Barrena, R. Mysyk, Review on supercapacitors: technologies and materials. *Renew. Sustain. Energy Rev.* **58**, 1189–1206 (2016). <https://doi.org/10.1016/j.rser.2015.12.249>
 18. A. Berrueta, A. Ursúa, I. San Martín, A. Eftekhari, P. Sanchis, Supercapacitors: electrical characteristics, modeling, applications, and future trends. *IEEE Access* **7**, 50869–50896 (2019). <https://doi.org/10.1109/ACCESS.2019.2908558>
 19. J. Wang, J. Wang, Z. Kong, K. Lv, C. Teng, Y. Zhu, Conducting-polymer-based materials for electrochemical energy conversion and storage. *Adv. Mater.* **29**(45), 1703044 (2017). <https://doi.org/10.1002/adma.201703044>
 20. W. Raza, F. Ali, N. Raza, Y. Luo, K.-H. Kim, J. Yang, S. Kumar, A. Mehmood, E.E. Kwon, Recent advancements in supercapacitor technology. *Nano Energy* **52**, 441–473 (2018). <https://doi.org/10.1016/j.nanoen.2018.08.013>
 21. Z. Qiu, Y. Wang, X. Bi, T. Zhou, J. Zhou, J. Zhao, Z. Miao, W. Yi, P. Fu, S. Zhuo, Biochar-based carbons with hierarchical micro-meso-macro porosity for high rate and long cycle life supercapacitors. *J. Power Sources* **376**, 82–90 (2018). <https://doi.org/10.1016/j.jpowsour.2017.11.077>
 22. K. Ren, Z. Liu, T. Wei, Z. Fan, Recent developments of transition metal compounds-carbon hybrid electrodes for high energy/power supercapacitors. *Nano-Micro Lett.* **13**(1), 1–32 (2021). <https://doi.org/10.1007/s40820-021-00642-2>
 23. P. Veerakumar, A. Sangili, S. Manavalan, P. Thanasekaran, K.-C. Lin, Research progress on porous carbon supported metal/metal oxide nanomaterials for supercapacitor electrode applications. *Ind. Eng. Chem. Res.* **59**(14), 6347–6374 (2020). <https://doi.org/10.1021/acs.iecr.9b06010>
 24. K.A. Owusu, L. Qu, J. Li, Z. Wang, K. Zhao, C. Yang, K.M. Hercule, C. Lin, C. Shi, Q. Wei, Low-crystalline iron oxide hydroxide nanoparticle anode for high-performance supercapacitors. *Nat. Commun.* **8**(1), 1–11 (2017). <https://doi.org/10.1038/ncomms14264>
 25. L. Zheng, J. Song, X. Ye, Y. Wang, X. Shi, H. Zheng, Construction of self-supported hierarchical NiCo-S nanosheet arrays for supercapacitors with ultrahigh specific capacitance. *Nanoscale* **12**(25), 13811–13821 (2020). <https://doi.org/10.1039/D0NR02976A>
 26. P. Geng, S. Zheng, H. Tang, R. Zhu, L. Zhang, S. Cao, H. Xue, H. Pang, Transition metal sulfides based on graphene for electrochemical energy storage. *Adv. Energy Mater.* **8**(15), 1703259 (2018)
 27. Y. Wang, Y. Song, Y. Xia, Electrochemical capacitors: mechanism, materials, systems, characterization and applications. *Chem. Soc. Rev.* **45**(21), 5925–5950 (2016). <https://doi.org/10.1039/C5CS00580A>
 28. H. Liu, X. Liu, S. Wang, H.-K. Liu, L. Li, Transition metal based battery-type electrodes in hybrid supercapacitors: a review. *Energy Storage Materials* **28**, 122–145 (2020). <https://doi.org/10.1016/j.ensm.2020.03.003>
 29. L. Hou, W. Yang, R. Li, X. Xu, P. Wang, B. Deng, F. Yang, Y. Li, Self-reconstruction strategy to synthesis of Ni/Co-OOH nanoflowers decorated with N, S co-doped carbon for high-performance energy storage. *Chem. Eng. J.* **396**, 125323 (2020). <https://doi.org/10.1016/j.cej.2020.125323>
 30. Y. Son, M. Park, Y. Son, J.-S. Lee, J.-H. Jang, Y. Kim, J. Cho, Quantum confinement and its related effects on the critical size of GeO₂ nanoparticles anodes for lithium batteries. *Nano Lett.* **14**(2), 1005–1010 (2014). <https://doi.org/10.1021/nl404466v>
 31. R. Mo, Z. Lei, K. Sun, D. Rooney, Facile synthesis of anatase TiO₂ quantum-dot/graphene-nanosheet composites with enhanced electrochemical performance for lithium-ion batteries. *Adv. Mater.* **26**(13), 2084–2088 (2014). <https://doi.org/10.1002/adma.201304338>
 32. H. Xia, C. Hong, B. Li, B. Zhao, Z. Lin, M. Zheng, S.V. Savilov, S.M. Aldoshin, Facile synthesis of hematite quantum-dot/functionalized graphene-sheet composites as advanced anode materials for asymmetric supercapacitors. *Adv. Func. Mater.* **25**(4), 627–635 (2015). <https://doi.org/10.1002/adfm.201403554>
 33. H.M. Jeong, K.M. Choi, T. Cheng, D.K. Lee, R. Zhou, I.W. Ock, D.J. Milliron, W.A. Goddard, J.K. Kang, Rescaling of metal oxide nanocrystals for energy storage having high capacitance and energy density with robust cycle life. *Proc. Natl. Acad. Sci. U.S.A.* **112**(26), 7914–7919 (2015). <https://doi.org/10.1073/pnas.1503546112>
 34. N. Agnihotri, P. Sen, A. De, M. Mukherjee, Hierarchically designed PEDOT encapsulated graphene-MnO₂ nanocomposite as supercapacitors. *Mater. Res. Bull.* **88**, 218–225 (2017). <https://doi.org/10.1016/j.materresbull.2016.12.036>
 35. G. Wang, Z. Jin, Q. Guo, Ordered self-supporting NiV LDHs@P-nickel foam nano-array as high-performance supercapacitor electrode. *J. Colloid Interface Sci.* **583**, 1–12 (2021). <https://doi.org/10.1016/j.jcis.2020.08.127>
 36. G. Zhang, T. Wu, H. Zhou, H. Jin, K. Liu, Y. Luo, H. Jiang, K. Huang, L. Huang, J. Zhou, Rich alkali ions preintercalated vanadium oxides for durable and fast zinc-ion storage. *ACS Energy Lett.* **6**(6), 2111–2120 (2021). <https://doi.org/10.1021/acscenergyl.1c00625>
 37. W. Wu, L. Yang, S. Chen, Y. Shao, L. Jing, G. Zhao, H. Wei, Core-shell nanospherical polypyrrole/graphene oxide composites for high performance supercapacitors. *RSC Adv.* **5**(111), 91645–91653 (2015). <https://doi.org/10.1039/C5RA17036B>
 38. Z. Wang, Y. Long, D. Cao, D. Han, F. Gu, A high-performance flexible supercapacitor based on hierarchical Co₃O₄-SnO₂@SnO₂ nanostructures. *Electrochim. Acta* **307**, 341–350 (2019). <https://doi.org/10.1016/j.electacta.2019.03.230>

39. M. Chaudhary, M. Singh, A. Kumar, Prachi, Y.K. Gautam, A.K. Malik, Y. Kumar, and B.P. Singh, Experimental investigation of Co and Fe-Doped CuO nanostructured electrode material for remarkable electrochemical performance. *Ceram. Int.* **47**(2), 2094–2106. (2021). <https://doi.org/10.1016/j.ceramint.2020.09.042>.
40. J. Wan, X. Yao, X. Gao, X. Xiao, T. Li, J. Wu, W. Sun, Z. Hu, H. Yu, L. Huang, M. Liu, J. Zhou, Microwave combustion for modification of transition metal oxides. *Adv. Func. Mater.* **26**(40), 7263–7270 (2016). <https://doi.org/10.1002/adfm.201603125>
41. A.C. Nwanya, D. Obi, K.I. Ozoemena, R.U. Osuji, C. Awada, A. Ruediger, M. Maaza, F. Rosei, F.I. Ezema, Facile synthesis of nanosheet-like CuO film and its potential application as a high-performance pseudocapacitor electrode. *Electrochim. Acta* **198**, 220–230 (2016). <https://doi.org/10.1016/j.electacta.2016.03.064>
42. S. Paulraj, R. Jayavel, Microwave-assisted synthesis of Ru and Ce doped tungsten oxide for supercapacitor electrodes. *J. Mater. Sci.: Mater. Electron.* **29**(16), 13794–13802 (2018). <https://doi.org/10.1007/s10854-018-9510-5>
43. Y. Wang, X. Li, Y. Wang, Y. Liu, Y. Bai, R. Liu, G. Yuan, High-performance flexible MnO₂@carbonized cotton textile electrodes for enlarged operating potential window symmetrical supercapacitors. *Electrochim. Acta* **299**, 12–18 (2019). <https://doi.org/10.1016/j.electacta.2018.12.181>
44. L. Cui, C. Cheng, F. Peng, Y. Yang, Y. Li, M. Jia, X. Jin, A ternary MnO₂-deposited RGO/lignin-based porous carbon composite electrode for flexible supercapacitor applications. *New J. Chem.* **43**(35), 14084–14092 (2019). <https://doi.org/10.1039/c9nj02184a>
45. M. Ghorbani, M.R. Golobostanfard, H. Abdizadeh, Flexible freestanding sandwich type ZnO/rGO/ZnO electrode for wearable supercapacitor. *Appl. Surf. Sci.* **419**, 277–285 (2017). <https://doi.org/10.1016/j.apsusc.2017.05.060>
46. Y. Guo, Z. Zhu, Y. Chen, H. He, X. Li, T. Qin, Y. Wang, High-performance supercapacitors of ruthenium-based nanohybrid compounds. *J. Alloy Compd.* **842**, 155798 (2020). <https://doi.org/10.1016/j.jallcom.2020.155798>
47. K.-C. Huang, C.-H. Lin, K.S. Anuratha, T.-Y. Huang, J.-Y. Lin, F.-G. Tseng, C.-K. Hsieh, Laser printer patterned sacrificed layer for arbitrary design and scalable fabrication of the all-solid-state interdigitated in-planar hydrous ruthenium oxide flexible micro supercapacitors. *J. Power Sources* **417**, 108–116 (2019). <https://doi.org/10.1016/j.jpowsour.2019.02.016>
48. S.N. Khatavkar, S.D. Sartale, α -Fe₂O₃ thin film on stainless steel mesh: a flexible electrode for supercapacitor. *Mater. Chem. Phys.* **225**, 284–291 (2019). <https://doi.org/10.1016/j.matchemphys.2018.12.079>
49. J. Shen, Q. Wang, K. Zhang, S. Wang, L. Li, S. Dong, S. Zhao, J. Chen, R. Sun, Y. Wang, Z. Jian, W. Zhang, Flexible carbon cloth based solid-state supercapacitor from hierarchical holothurian-morphological NiCo₂O₄@NiMoO₄/PANI. *Electrochim. Acta* **320**, 134578 (2019). <https://doi.org/10.1016/j.electacta.2019.134578>
50. S. Liu, Y. Yin, Y. Shen, K.S. Hui, Y.T. Chun, J.M. Kim, K.N. Hui, L. Zhang, S.C. Jun, Phosphorus regulated cobalt oxide@nitrogen-doped carbon nanowires for flexible quasi-solid-state supercapacitors. *Small* **16**(4), 1906458 (2020). <https://doi.org/10.1002/smll.201906458>
51. X. Li, Z. Yang, W. Qi, Y. Li, Y. Wu, S. Zhou, S. Huang, J. Wei, H. Li, P. Yao, Binder-free Co₃O₄@NiCoAl-layered double hydroxide core-shell hybrid architectural nanowire arrays with enhanced electrochemical performance. *Appl. Surf. Sci.* **363**, 381–388 (2016). <https://doi.org/10.1016/j.apsusc.2015.12.039>
52. S.C. Lee, M. Kim, J.-H. Park, E.S. Kim, S. Liu, K.Y. Chung, S. Chan Jun, An unexpected phase-transformation of cobalt–vanadium layered double hydroxides toward high energy density hybrid supercapacitor. *J Power Sources* **486**, 229–341 (2021). <https://doi.org/10.1016/j.jpowsour.2020.229341>
53. P.A. Shinde, N.R. Chodankar, S. Lee, E. Jung, S. Aftab, Y.-K. Han, S.C. Jun, All-redox solid-state supercapacitor with cobalt manganese oxide@bimetallic hydroxides and vanadium nitride@nitrogen-doped carbon electrodes. *Chem. Eng. J.* **405**, 127029 (2021). <https://doi.org/10.1016/j.cej.2020.127029>
54. X. Tang, X. Guo, W. Wu, G. Wang, 2D metal carbides and nitrides (MXenes) as high-performance electrode materials for Lithium-based batteries. *Adv. Energy Mater.* **8**(33), 1801897 (2018). <https://doi.org/10.1002/aenm.201801897>
55. C. Zhu, Y. Sun, D. Chao, X. Wang, P. Yang, X. Zhang, H. Huang, H. Zhang, H.J. Fan, A 2.0 V capacitive device derived from shape-preserved metal nitride nanorods. *Nano Energy* **26**, 1–6 (2016). <https://doi.org/10.1016/j.nanoen.2016.04.056>
56. Y. Zhang, B. Ouyang, J. Xu, G. Jia, S. Chen, R.S. Rawat, H.J. Fan, Rapid synthesis of cobalt nitride nanowires: highly efficient and low-cost catalysts for oxygen evolution. *Angew. Chem.* **128**(30), 8812–8816 (2016). <https://doi.org/10.1002/ange.201604372>
57. B. Gao, X. Li, K. Ding, C. Huang, Q. Li, P.K. Chu, K. Huo, Recent progress in nanostructured transition metal nitrides for advanced electrochemical energy storage. *J. Mater. Chem. A* **7**(1), 14–37 (2019). <https://doi.org/10.1039/C8TA05760E>
58. Y. Zhong, X. Xia, F. Shi, J. Zhan, J. Tu, H.J. Fan, Transition metal carbides and nitrides in energy storage and conversion. *Adv. Sci.* **3**(5), 150286 (2016)
59. M.-S. Balogun, Y. Huang, W. Qiu, H. Yang, H. Ji, Y. Tong, Updates on the development of nanostructured transition metal nitrides for electrochemical energy storage and water splitting. *Mater. Today* **20**(8), 425–451 (2017)
60. D. Choi, P.N. Kumta, Synthesis and characterization of nanostructured niobium and molybdenum nitrides by a two-step transition metal halide approach. *J. Am. Ceram. Soc.* **94**(8),

- 2371–2378 (2011). <https://doi.org/10.1111/j.1551-2916.2011.04412.x>
61. K. Schwarz, Band structure and chemical bonding in transition metal carbides and nitrides. *Crit. Rev. Solid State Mater. Sci.* **13**(3), 211–257 (1987). <https://doi.org/10.1080/10408438708242178>
 62. D.J. Ham, J.S. Lee, Transition metal carbides and nitrides as electrode materials for low temperature fuel cells. *Energies* **2**(4), 873–899 (2009). <https://doi.org/10.3390/en20400873>
 63. D. Zhao, Z. Cui, S. Wang, J. Qin, M. Cao, VN hollow spheres assembled from porous nanosheets for high-performance lithium storage and the oxygen reduction reaction. *J. Mater. Chem. A* **4**(20), 7914–7923 (2016). <https://doi.org/10.1039/C6TA01707J>
 64. C. Huang, Y. Yang, J. Fu, J. Wu, H. Song, X. Zhang, B. Gao, P.K. Chu, K. Huo, Flexible Nb₄N₅/rGO electrode for high-performance solid state supercapacitors. *J. Nanosci. Nanotechnol.* **18**(1), 30–38 (2018). <https://doi.org/10.1166/jnn.2018.14595>
 65. W. Bi, Z. Hu, X. Li, C. Wu, J. Wu, Y. Wu, Y. Xie, Metallic mesocrystal nanosheets of vanadium nitride for high-performance all-solid-state pseudocapacitors. *Nano Res.* **8**(1), 193–200 (2015). <https://doi.org/10.1007/s12274-014-0612-y>
 66. C. Dong, X. Wang, X. Liu, X. Yuan, W. Dong, H. Cui, Y. Duan, F. Huang, In situ grown Nb₄N₅ nanocrystal on nitrogen-doped graphene as a novel anode for lithium ion battery. *RSC Adv.* **6**(84), 81290–81295 (2016). <https://doi.org/10.1039/c6ra13647h>
 67. H. Xu, H. Zhang, L. Fang, J. Yang, K. Wu, Y. Wang, Hierarchical molybdenum nitride nanochexes by a textured self-assembly in gas–solid phase for the enhanced application in lithium ion batteries. *ACS Nano* **9**(7), 6817–6825 (2015). <https://doi.org/10.1021/acsnano.5b02415>
 68. B. Das, M. Behm, G. Lindbergh, M.V. Reddy, B.V.R. Chowdari, High performance metal nitrides, MN (M = Cr, Co) nanoparticles for non-aqueous hybrid supercapacitors. *Adv. Powder Technol.* **26**(3), 783–788 (2015). <https://doi.org/10.1016/j.appt.2015.02.001>
 69. X. Jiang, W. Lu, X. Yu, S. Song, Y. Xing, Fabrication of a vanadium nitride/N-doped carbon hollow nanosphere composite as an efficient electrode material for asymmetric supercapacitors. *Nanoscale Adv.* **2**(9), 3865–3871 (2020). <https://doi.org/10.1039/D0NA00288G>
 70. Z. Qi, B. Wei, J. Wang, Y. Yang, Z. Wang, Nanostructured porous CrN thin films by oblique angle magnetron sputtering for symmetric supercapacitors. *J. Alloy Compd.* **806**, 953–959 (2019). <https://doi.org/10.1016/j.jallcom.2019.07.325>
 71. A. Guerra, E. Haye, A. Achour, M. Harnois, T. Hadjersi, J.-F. Colomer, J.-J. Pireaux, S. Lucas, R. Boukherroub, High performance of 3D silicon nanowires array@CrN for electrochemical capacitors. *Nanotechnology* **31**(3), 035407 (2020). <https://doi.org/10.1088/1361-6528/ab4963>
 72. Z. Gao, Z. Wu, S. Zhao, T. Zhang, Q. Wang, Enhanced capacitive property of HfN film electrode by plasma etching for supercapacitors. *Mater. Lett.* **235**, 148–152 (2019). <https://doi.org/10.1016/j.matlet.2018.10.032>
 73. H. Shen, B. Wei, D. Zhang, Z. Qi, Z. Wang, Magnetron sputtered NbN thin film electrodes for supercapacitors. *Mater. Lett.* **229**, 17–20 (2018). <https://doi.org/10.1016/j.matlet.2018.06.052>
 74. T. He, W. Zhang, P. Manasa, F. Ran, Quantum dots of molybdenum nitride embedded in continuously distributed polyaniline as novel electrode material for supercapacitor. *J. Alloy Compd.* **812**, 152138 (2020). <https://doi.org/10.1016/j.jallcom.2019.152138>
 75. S. Ouendi, K. Robert, D. Stiévenard, T. Brousse, P. Roussel, C. Lethien, Sputtered tungsten nitride films as pseudocapacitive electrode for on chip micro-supercapacitors. *Energy Storage Mater.* **20**, 243–252 (2019). <https://doi.org/10.1016/j.ensm.2019.04.006>
 76. X. Xu, S. Chang, Z. Hong, Y. Zeng, H. Zhang, P. Li, S. Zheng, Z. Wang, S. Duo, Construction of 3D CrN@ nitrogen-doped carbon nanosheet arrays by reactive magnetron sputtering for the free-standing electrode of supercapacitor. *Nanotechnology* **33**(5), 055402 (2021). <https://doi.org/10.1088/1361-6528/ac3356>
 77. S. Venkateshalu, J. Cherusseri, M. Karnan, K.S. Kumar, P. Kollu, M. Sathish, J. Thomas, S.K. Jeong, A.N. Grace, New method for the synthesis of 2D vanadium nitride (MXene) and its application as a supercapacitor electrode. *ACS Omega* **5**(29), 17983–17992 (2020). <https://doi.org/10.1021/acsomega.0c01215>
 78. L. Xu, L. Sun, J. Feng, L. Qi, I. Muhammad, J. Maher, X. Cheng, W. Song, Nanocasting synthesis of an iron nitride-ordered mesopore carbon composite as a novel electrode material for supercapacitors. *RSC Adv.* **7**(70), 44619–44625 (2017). <https://doi.org/10.1039/c7ra08704g>
 79. A. Śliwak, A. Moysowicz, G. Grylewicz, Hydrothermal-assisted synthesis of an iron nitride–carbon composite as a novel electrode material for supercapacitors. *J. Mater. Chem. A* **5**(12), 5680–5684 (2017). <https://doi.org/10.1039/C6TA10985C>
 80. M. Ishaq, M. Jabeen, W. Song, L. Xu, W. Li, Q. Deng, Fluorinated graphene-supported Nickel–Cobalt–Iron nitride nanoparticles as a promising hybrid electrode for supercapacitor applications. *Electrochim. Acta* **282**, 913–922 (2018). <https://doi.org/10.1016/j.electacta.2018.06.087>
 81. N. Ouldhamadouche, A. Achour, R. Lucio-Porto, M. Islam, S. Solaymani, A. Arman, A. Ahmadpourian, H. Achour, L. Le Brizoual, M.A. Djouadi, Electrodes based on nano-tree-like vanadium nitride and carbon nanotubes for micro-supercapacitors. *J. Mater. Sci. Technol.* **34**(6), 976–982 (2018). <https://doi.org/10.1016/j.jmst.2017.11.048>

82. W. Zhang, Y. Yang, M. Ravi, L. Kong, L. Kang, F. Ran, Interconnected porous composites electrode materials of Carbon@ Vanadium nitride by directly absorbing VO₃. *Electrochim. Acta* **306**, 113–121 (2019). <https://doi.org/10.1016/j.electacta.2019.03.112>
83. A. Salman, S. Padmajan Sasikala, I.H. Kim, J.T. Kim, G.S. Lee, J.G. Kim, S.O. Kim, Tungsten nitride-coated graphene fibers for high-performance wearable supercapacitors. *Nanoscale* **12**(39), 20239–20249 (2020). <https://doi.org/10.1039/d0nr06636b>
84. J. Wang, K. Ma, J. Zhang, F. Liu, J. Cheng, Template-free synthesis of hierarchical hollow NiS_x microspheres for supercapacitor. *J. Colloid Interface Sci.* **507**, 290–299 (2017). <https://doi.org/10.1016/j.jcis.2017.07.095>
85. Q. Zhang, L. Mei, X. Cao, Y. Tang, Z. Zeng, Intercalation and exfoliation chemistries of transition metal dichalcogenides. *J. Mater. Chem. A* **8**(31), 15417–15444 (2020). <https://doi.org/10.1039/D0TA03727C>
86. H. Tong, W. Bai, S. Yue, Z. Gao, L. Lu, L. Shen, S. Dong, J. Zhu, J. He, X. Zhang, Zinc cobalt sulfide nanosheets grown on nitrogen-doped graphene/carbon nanotube film as a high-performance electrode for supercapacitors. *J. Mater. Chem. A* **4**(29), 11256–11263 (2016). <https://doi.org/10.1039/C6TA02249A>
87. P. Kulkarni, S. Nataraj, R.G. Balakrishna, D. Nagaraju, M. Reddy, Nanostructured binary and ternary metal sulfides: synthesis methods and their application in energy conversion and storage devices. *J. Mater. Chem. A* **5**(42), 22040–22094 (2017). <https://doi.org/10.1039/C7TA07329A>
88. T. Li, Y. Bai, Y. Wang, H. Xu, H. Jin, Advances in transition-metal (Zn, Mn, Cu)-based MOFs and their derivatives for anode of lithium-ion batteries. *Coord. Chem. Rev.* **410**, 213221 (2020). <https://doi.org/10.1016/j.ccr.2020.213221>
89. Z. Zhang, Z. Huang, L. Ren, Y. Shen, X. Qi, J. Zhong, One-pot synthesis of hierarchically nanostructured Ni₃S₂ dendrites as active materials for supercapacitors. *Electrochim. Acta* **149**, 316–323 (2014). <https://doi.org/10.1016/j.electacta.2014.10.097>
90. D. Kim, P. Karthick Kannan, S. Mateti, C.-H. Chung, Indirect nanoconstruction morphology of Ni₃S₂ electrodes renovates the performance for electrochemical energy storage. *ACS Appl. Energy Mater.* **1**(12), 6945–6952 (2018). <https://doi.org/10.1021/acsaem.8b01310>
91. T. Chen, Z. Liu, Z. Liu, X. Tao, H. Fan, L. Guo, Fabrication of interconnected 2D/3D NiS/Ni₃S₄ composites for high performance supercapacitor. *Mater. Lett.* **248**, 1–4 (2019). <https://doi.org/10.1016/j.matlet.2019.03.125>
92. S. Liu, K. San Hui, K.N. Hui, J.M. Yun, K.H. Kim, Vertically stacked bilayer CuCo₂O₄/MnCo₂O₄ heterostructures on functionalized graphite paper for high-performance electrochemical capacitors. *J. Mater. Chem. A* **4**(21), 8061–8071 (2016). <https://doi.org/10.1039/C6TA00960C>
93. J. Ren, Q. Meng, Z. Xu, X. Zhang, J. Chen, CoS₂ hollow nanocubes derived from Co-Co Prussian blue analogue: High-performance electrode materials for supercapacitors. *J. Electroanal. Chem.* **836**, 30–37 (2019). <https://doi.org/10.1016/j.jelechem.2019.01.049>
94. H. Jia, Z. Wang, X. Zheng, Y. Cai, J. Lin, H. Liang, J. Qi, J. Cao, J. Feng, W. Fei, Controlled synthesis of MOF-derived quadruple-shelled CoS₂ hollow dodecahedrons as enhanced electrodes for supercapacitors. *Electrochim. Acta* **312**, 54–61 (2019). <https://doi.org/10.1016/j.electacta.2019.04.192>
95. Z. Sun, X. Yang, H. Lin, F. Zhang, Q. Wang, F. Qu, Bifunctional iron disulfide nanoellipsoids for high energy density supercapacitor and electrocatalytic oxygen evolution applications. *Inorg. Chem. Front.* **6**(3), 659–670 (2019). <https://doi.org/10.1039/C8QI01230J>
96. D. Li, S. Song, J. Lu, J. Liang, Y. Zhang, L. Li, A general self-template-etched solution route for the synthesis of 2D γ -manganese sulfide nanoplates and their enhanced supercapacitive performance. *New J. Chem.* **43**(12), 4674–4680 (2019). <https://doi.org/10.1039/C8NJ06143B>
97. R.K. Mishra, G.W. Baek, K. Kim, H.-I. Kwon, S.H. Jin, One-step solvothermal synthesis of carnation flower-like SnS₂ as superior electrodes for supercapacitor applications. *Appl. Surf. Sci.* **425**, 923–931 (2017). <https://doi.org/10.1016/j.apsusc.2017.07.045>
98. N. Parveen, S.A. Ansari, H.R. Alamri, M.O. Ansari, Z. Khan, M.H. Cho, Facile synthesis of SnS₂ nanostructures with different morphologies for high-performance supercapacitor applications. *ACS Omega* **3**(2), 1581–1588 (2018). <https://doi.org/10.1021/acsomega.7b01939>
99. X.Y. Yu, X.W. David Lou, Mixed metal sulfides for electrochemical energy storage and conversion. *Adv. Energy Mater.* **8**(3), 1701–592 (2018). <https://doi.org/10.1002/aenm.201701592>
100. R. Xu, J. Lin, J. Wu, M. Huang, L. Fan, X. He, Y. Wang, Z. Xu, A two-step hydrothermal synthesis approach to synthesize NiCo₂S₄/NiS hollow nanospheres for high-performance asymmetric supercapacitors. *Appl. Surf. Sci.* **422**, 597–606 (2017). <https://doi.org/10.1016/j.apsusc.2017.06.003>
101. B.Y. Guan, L. Yu, X. Wang, S. Song, X.W.D. Lou, Formation of onion-like NiCo₂S₄ particles via sequential ion-exchange for hybrid supercapacitors. *Adv. Mater.* **29**(6), 1605051 (2017). <https://doi.org/10.1002/adma.201605051>
102. M. Govindasamy, S. Shanthi, E. Elaiyappillai, S.-F. Wang, P.M. Johnson, H. Ikeda, Y. Hayakawa, S. Ponnusamy, C. Muthamizhchelvan, Fabrication of hierarchical NiCo₂S₄@ CoS₂ nanostructures on highly conductive flexible carbon cloth substrate as a hybrid electrode material for supercapacitors with enhanced electrochemical performance. *Electrochim. Acta* **293**, 328–337 (2019). <https://doi.org/10.1016/j.electacta.2018.10.051>
103. S. Yu, V.M.H. Ng, F. Wang, Z. Xiao, C. Li, L.B. Kong, W. Que, K. Zhou, Synthesis and application of iron-based nanomaterials as

- anodes of lithium-ion batteries and supercapacitors. *J. Mater. Chem. A* **6**(20), 9332–9367 (2018).
104. B. Balakrishnan, S.K. Balasingam, K. SivalingamNallathambi, A. Ramadoss, M. Kundu, J.S. Bak, I.H. Cho, P. Kandasamy, Y. Jun, H.-J. Kim, Facile synthesis of pristine FeS₂ microflowers and hybrid rGO-FeS₂ microsphere electrode materials for high performance symmetric capacitors. *J. Ind. Eng. Chem.* **71**, 191–200 (2019). <https://doi.org/10.1016/j.jiec.2018.11.022>
 105. A.M. Zardkhoui, S.S.H. Davarani, A.A. Asgharinezhad, Designing graphene-wrapped NiCo₂Se₄ microspheres with petal-like FeS₂ toward flexible asymmetric all-solid-state supercapacitors. *Dalton Trans.* **48**(13), 4274–4282 (2019). <https://doi.org/10.1039/C9DT00009G>
 106. P. Naveenkumar, G.P. Kalaigan, Electrodeposited MnS on graphene wrapped Ni-Foam for enhanced supercapacitor applications. *Electrochim. Acta* **289**, 437–447 (2018). <https://doi.org/10.1016/j.electacta.2018.09.100>
 107. X. Xu, X. Zhang, Y. Zhao, Y. Hu, An efficient hybrid supercapacitor based on battery-type MnS/reduced graphene oxide and capacitor-type biomass derived activated carbon. *J. Mater. Sci.: Mater. Electron.* **29**(10), 8410–8420 (2018). <https://doi.org/10.1007/s10854-018-8852-3>
 108. R. Barik, N. Devi, V.K. Perla, S.K. Ghosh, K. Mallick, Stannous sulfide nanoparticles for supercapacitor application. *Appl. Surf. Sci.* **472**, 112–117 (2019). <https://doi.org/10.1016/j.apsusc.2018.03.172>
 109. J.N. Coleman, M. Lotya, A. O'Neill, S.D. Bergin, P.J. King, U. Khan, K. Young, A. Gaucher, S. De, R.J. Smith, Two-dimensional nanosheets produced by liquid exfoliation of layered materials. *Science* **331**(6017), 568–571 (2011). <https://doi.org/10.1126/science.1194975>
 110. M. Sajjad, W. Lu, Covalent organic frameworks based nanomaterials: design, synthesis, and current status for supercapacitor applications: a review. *J. Energy Storage* **39**, 102618 (2021). <https://doi.org/10.1016/j.est.2021.102618>
 111. N.S. Arul, J.I. Han, Facile hydrothermal synthesis of hexapod-like two dimensional dichalcogenide NiSe₂ for supercapacitor. *Mater. Lett.* **181**, 345–349 (2016). <https://doi.org/10.1016/j.matlet.2016.06.065>
 112. Y. Gu, W. Du, Y. Darrat, M. Saleh, Y. Huang, Z. Zhang, S. Wei, In situ growth of novel nickel diselenide nanoarrays with high specific capacity as the electrode material of flexible hybrid supercapacitors. *Appl. Nanosci.* **10**(5), 1591–1601 (2019). <https://doi.org/10.1007/s13204-019-01234-8>
 113. P. Pazhamalai, K. Krishnamoorthy, S. Sahoo, S.J. Kim, Two-dimensional molybdenum diselenide nanosheets as a novel electrode material for symmetric supercapacitors using organic electrolyte. *Electrochim. Acta* **295**, 591–598 (2019). <https://doi.org/10.1016/j.electacta.2018.10.191>
 114. Y. Gu, L.-Q. Fan, J.-L. Huang, C.-L. Geng, J.-M. Lin, M.-L. Huang, Y.-F. Huang, J.-H. Wu, N-doped reduced graphene oxide decorated NiSe₂ nanoparticles for high-performance asymmetric supercapacitors. *J. Power Sources* **425**, 60–68 (2019). <https://doi.org/10.1016/j.jpowsour.2019.03.123>
 115. A. Gopalakrishnan, S. Badhulika, Binder-free polyaniline sheathed crumpled cobalt diselenide nanoparticles as an advanced electrode for high specific energy asymmetric supercapacitor. *J. Energy Storage* **41**, 102853 (2021). <https://doi.org/10.1016/j.est.2021.102853>
 116. C. Miao, X. Yin, G. Xia, K. Zhu, K. Ye, Q. Wang, J. Yan, D. Cao, G. Wang, Facile microwave-assisted synthesis of cobalt diselenide/reduced graphene oxide composite for high-performance supercapacitors. *Appl. Surf. Sci.* **543**, 148811 (2021). <https://doi.org/10.1016/j.apsusc.2020.148811>
 117. C. Miao, X. Xiao, Y. Gong, K. Zhu, K. Cheng, K. Ye, J. Yan, D. Cao, G. Wang, P. Xu, Facile synthesis of metal-organic framework-derived CoSe₂ nanoparticles embedded in the N-doped carbon nanosheet array and application for supercapacitors. *ACS Appl. Mater. Interfaces.* **12**(8), 9365–9375 (2020). <https://doi.org/10.1021/acsami.9b22606>
 118. C.V.V.M. Gopi, A.E. Reddy, J.-S. Bak, I.-H. Cho, H.-J. Kim, One-pot hydrothermal synthesis of tungsten diselenide/reduced graphene oxide composite as advanced electrode materials for supercapacitors. *Mater. Lett.* **223**, 57–60 (2018). <https://doi.org/10.1016/j.matlet.2018.04.023>
 119. S.R. Marri, S. Ratha, C.S. Rout, J. Behera, 3D cuboidal vanadium diselenide embedded reduced graphene oxide hybrid structures with enhanced supercapacitor properties. *Chem. Commun.* **53**(1), 228–231 (2017). <https://doi.org/10.1039/C6CC08035A>
 120. H.M. El Sharkawy, D.M. Sayed, A.S. Dhmees, R.M. Aboushahba, N.K. Allam, Facile synthesis of nanostructured binary Ni-Cu phosphides as advanced battery materials for asymmetric electrochemical supercapacitors. *ACS Appl. Energy Mater.* **3**(9), 9305–9314 (2020). <https://doi.org/10.1021/acsaem.0c01630>
 121. X. Li, A.M. Elshahawy, C. Guan, J. Wang, Metal phosphides and phosphates-based electrodes for electrochemical supercapacitors. *Small* **13**(39), 1701530 (2017). <https://doi.org/10.1002/sml.201701530>
 122. J. Theerthagiri, A.P. Murthy, S.J. Lee, K. Karuppasamy, S.R. Arumugam, Y. Yu, M.M. Hanafiah, H.-S. Kim, V. Mittal, M.Y. Choi, Recent progress on synthetic strategies and applications of transition metal phosphides in energy storage and conversion. *Ceram. Int.* **47**(4), 4404–4425 (2021). <https://doi.org/10.1016/j.ceramint.2020.10.098>
 123. Y.-C. Chen, Z.-B. Chen, Y.-G. Lin, Y.-K. Hsu, Synthesis of copper phosphide nanotube arrays as electrodes for asymmetric supercapacitors. *ACS Sustain. Chem. Eng.* **5**(5), 3863–3870 (2017). <https://doi.org/10.1021/acssuschemeng.6b03006>
 124. F. Liang, L. Huang, L. Tian, J. Li, H. Zhang, S. Zhang, Microwave-assisted hydrothermal synthesis of cobalt phosphide nanostructures for advanced supercapacitor electrodes.

- CrystEngComm **20**(17), 2413–2420 (2018). <https://doi.org/10.1039/c8ce00054a>
125. Z. Zheng, M. Retana, X. Hu, R. Luna, Y.H. Ikuhara, W. Zhou, Three-dimensional cobalt phosphide nanowire arrays as negative electrode material for flexible solid-state asymmetric supercapacitors. *ACS Appl. Mater. Interfaces*. **9**(20), 16986–16994 (2017). <https://doi.org/10.1021/acsmi.7b01109>
 126. G. Zhu, L. Yang, W. Wang, M. Ma, J. Zhang, H. Wen, D. Zheng, Y. Yao, Hierarchical three-dimensional manganese doped cobalt phosphide nanowire decorated nanosheet cluster arrays for high-performance electrochemical pseudocapacitor electrodes. *Chem. Commun.* **54**(66), 9234–9237 (2018). <https://doi.org/10.1039/C8CC02475H>
 127. MSP, S., G. Gnanasekaran, P. Pazhamalai, S. Sahoo, M.M. Hos-sain, R.M. Bhattarai, S.-J. Kim, and Y.S. Mok, *Hierarchically porous nanostructured nickel phosphide with carbon particles embedded by dielectric barrier discharge plasma deposition as a binder-free electrode for hybrid supercapacitors*. *ACS Sustainable Chemistry & Engineering*, 2019. **7**(17): p. 14805–14814. Doi: <https://doi.org/10.1021/acsschemeng.9b02832>.
 128. P. Sivakumar, M.G. Jung, C.J. Raj, H.H. Rana, H.S. Park, 1D interconnected porous binary transition metal phosphide nanowires for high performance hybrid supercapacitors. *Int. J. Energy Res.* (2021). <https://doi.org/10.1002/er.6874>
 129. S. Li, M. Hua, Y. Yang, W. Huang, X. Lin, L. Ci, J. Lou, P. Si, Self-supported multidimensional Ni–Fe phosphide networks with holey nanosheets for high-performance all-solid-state supercapacitors. *J. Mater. Chem. A* **7**(29), 17386–17399 (2019). <https://doi.org/10.1039/C9TA04832D>
 130. T.T. Nguyen, J. Balamurugan, N.H. Kim, J.H. Lee, Hierarchical 3D Zn–Ni–P nanosheet arrays as an advanced electrode for high-performance all-solid-state asymmetric supercapacitors. *J. Mater. Chem. A* **6**(18), 8669–8681 (2018). <https://doi.org/10.1039/C8TA01184B>
 131. A.A. Saleh, A. Amer, D.M. Sayed, N.K. Allam, A facile electro-synthesis approach of Mn–Ni–Co ternary phosphides as binder-free active electrode materials for high-performance electrochemical supercapacitors. *Electrochim. Acta* **380**, 138197 (2021). <https://doi.org/10.1016/j.electacta.2021.138197>
 132. D. Ling, N. Lee, T. Hyeon, Chemical synthesis and assembly of uniformly sized iron oxide nanoparticles for medical applications. *Acc. Chem. Res.* **48**(5), 1276–1285 (2015). <https://doi.org/10.1021/acs.accounts.5b00038>
 133. S. Bai, H. Zou, H. Dietsch, Y.C. Simon, C. Weder, Functional iron oxide nanoparticles as reversible crosslinks for magnetically addressable shape-memory polymers. *Macromol. Chem. Phys.* **215**(5), 398–404 (2014). <https://doi.org/10.1002/macp.201300632>
 134. B. Šljukić, C.E. Banks, R.G. Compton, Iron oxide particles are the active sites for hydrogen peroxide sensing at multiwalled carbon nanotube modified electrodes. *Nano Lett.* **6**(7), 1556–1558 (2006). <https://doi.org/10.1021/nl060366v>
 135. G. Li, R. Li, W. Zhou, A wire-shaped supercapacitor in micrometer size based on Fe₃O₄ nanosheet arrays on Fe wire. *Nano-Micro Lett.* **9**(4), 1–8 (2017). <https://doi.org/10.1007/s40820-017-0147-3>
 136. T. Valdés-Solís, P. Valle-Vigón, S. Álvarez, G. Marbán, A.B. Fuertes, Manganese ferrite nanoparticles synthesized through a nanocasting route as a highly active Fenton catalyst. *Catal. Commun.* **8**(12), 2037–2042 (2007). <https://doi.org/10.1016/j.catcom.2007.03.030>
 137. E. Peng, E.S.G. Choo, P. Chandrasekharan, C.T. Yang, J. Ding, K.H. Chuang, J.M. Xue, Synthesis of manganese ferrite/graphene oxide nanocomposites for biomedical applications. *Small* **8**(23), 3620–3630 (2012). <https://doi.org/10.1002/smll.201201427>
 138. Z. Li, S.X. Wang, Q. Sun, H.L. Zhao, H. Lei, M.B. Lan, Z.X. Cheng, X.L. Wang, S.X. Dou, G.Q. Lu, Ultrasmall manganese ferrite nanoparticles as positive contrast agent for magnetic resonance imaging. *Adv. Healthcare Mater.* **2**(7), 958–964 (2013). <https://doi.org/10.1002/adhm.201200340>
 139. M.S. Amulya, H. Nagaswarupa, M.A. Kumar, C. Ravikumar, S. Prashantha, K. Kusuma, Sonochemical synthesis of NiFe₂O₄ nanoparticles: Characterization and their photocatalytic and electrochemical applications. *Appl. Surf. Sci. Adv.* **1**, 100023 (2020). <https://doi.org/10.1016/j.apsadv.2020.100023>
 140. S. Sharifi, A. Yazdani, K. Rahimi, Incremental substitution of Ni with Mn in NiFe₂O₄ to largely enhance its supercapacitance properties. *Sci. Rep.* **10**(1), 10916 (2020). <https://doi.org/10.1038/s41598-020-67802-z>
 141. B. Bhujun, M.T. Tan, A.S. Shanmugam, Study of mixed ternary transition metal ferrites as potential electrodes for supercapacitor applications. *Results Phys.* **7**, 345–353 (2017). <https://doi.org/10.1016/j.rinp.2016.04.010>
 142. A.A. Tahir, H.A. Burch, K.U. Wijayantha, B.G. Pollet, A new route to control texture of materials: Nanostructured ZnFe₂O₄ photoelectrodes. *Int. J. Hydrogen Energy* **38**(11), 4315–4323 (2013). <https://doi.org/10.1016/j.ijhydene.2013.01.130>
 143. A.A. Tahir, K.U. Wijayantha, Photoelectrochemical water splitting at nanostructured ZnFe₂O₄ electrodes. *J. Photochem. Photobiol. A* **216**(2–3), 119–125 (2010). <https://doi.org/10.1016/j.jphotochem.2010.07.032>
 144. N.K. Sahu, J. Gupta, D. Bahadur, PEGylated FePt–Fe₃O₄ composite nanoassemblies (CNAs): in vitro hyperthermia, drug delivery and generation of reactive oxygen species (ROS). *Dalton Trans.* **44**(19), 9103–9113 (2015). <https://doi.org/10.1039/C4DT03470H>
 145. S.S. Raut, B.R. Sankapal, First report on synthesis of ZnFe₂O₄ thin film using successive ionic layer adsorption and reaction: approach towards solid-state symmetric supercapacitor device.

- Electrochim. Acta **198**, 203–211 (2016). <https://doi.org/10.1016/j.electacta.2016.03.059>
146. V. Blanco-Gutierrez, R. Saez-Puche, M.J. Torralvo-Fernandez, Superparamagnetism and interparticle interactions in ZnFe₂O₄ nanocrystals. *J. Mater. Chem.* **22**(7), 2992–3003 (2012). <https://doi.org/10.1039/C1JM14856G>
 147. P. Guo, G. Zhang, J. Yu, H. Li, X. Zhao, Controlled synthesis, magnetic and photocatalytic properties of hollow spheres and colloidal nanocrystal clusters of manganese ferrite. *Colloids Surf., A* **395**, 168–174 (2012). <https://doi.org/10.1016/j.colsurfa.2011.12.027>
 148. J. Wang, Q. Chen, B. Hou, Z. Peng, Synthesis and magnetic properties of single-crystals of MnFe₂O₄ nanorods. *Eur. J. Inorg. Chem.* **2004**(6), 1165–1168 (2004). <https://doi.org/10.1002/ejic.200300555>
 149. H.-M. Fan, J.-B. Yi, Y. Yang, K.-W. Kho, H.-R. Tan, Z.-X. Shen, J. Ding, X.-W. Sun, M.C. Olivo, Y.-P. Feng, Single-crystalline MFe₂O₄ nanotubes/nanorings synthesized by thermal transformation process for biological applications. *ACS Nano* **3**(9), 2798–2808 (2009). <https://doi.org/10.1021/nn9006797>
 150. L. Cui, P. Guo, G. Zhang, Q. Li, R. Wang, M. Zhou, L. Ran, X. Zhao, Facile synthesis of cobalt ferrite submicrospheres with tunable magnetic and electrocatalytic properties. *Colloids Surf., A* **423**, 170–177 (2013). <https://doi.org/10.1016/j.colsurfa.2013.01.064>
 151. N. Bao, L. Shen, Y.-H.A. Wang, J. Ma, D. Mazumdar, A. Gupta, Controlled growth of monodisperse self-supported superparamagnetic nanostructures of spherical and rod-like CoFe₂O₄ nanocrystals. *J. Am. Chem. Soc.* **131**(36), 12900–12901 (2009). <https://doi.org/10.1021/ja905811h>
 152. Y. Xu, J. Wei, J. Yao, J. Fu, D. Xue, Synthesis of CoFe₂O₄ nanotube arrays through an improved sol–gel template approach. *Mater. Lett.* **62**(8–9), 1403–1405 (2008). <https://doi.org/10.1016/j.matlet.2007.08.066>
 153. S. Zhang, D. Dong, Y. Sui, Z. Liu, H. Wang, Z. Qian, W. Su, Preparation of core shell particles consisting of cobalt ferrite and silica by sol–gel process. *J. Alloy Compd.* **415**(1–2), 257–260 (2006). <https://doi.org/10.1016/j.jallcom.2005.07.048>
 154. H. Aijun, L. Juanjuan, Y. Mingquan, L. Yan, P. Xinhua, Preparation of nano-MnFe₂O₄ and its catalytic performance of thermal decomposition of ammonium perchlorate. *Chin. J. Chem. Eng.* **19**(6), 1047–1051 (2011). [https://doi.org/10.1016/S1004-9541\(11\)60090-6](https://doi.org/10.1016/S1004-9541(11)60090-6)
 155. S. Sartale, C. Lokhande, A room temperature two-step electrochemical process for large area nanocrystalline ferrite thin films deposition. *J. Electroceram.* **15**(1), 35–44 (2005). <https://doi.org/10.1007/s10832-005-1076-y>
 156. V. Vignesh, K. Subramani, M. Sathish, R. Navamathavan, Electrochemical investigation of manganese ferrites prepared via a facile synthesis route for supercapacitor applications. *Colloids Surf., A* **538**, 668–677 (2018). <https://doi.org/10.1016/j.colsurfa.2017.11.045>
 157. R. Roshani, A. Tadjarodi, Synthesis of ZnFe₂O₄ nanoparticles with high specific surface area for high-performance supercapacitor. *J. Mater. Sci.: Mater. Electron.* **31**(24), 23025–23036 (2020). <https://doi.org/10.1007/s10854-020-04830-5>
 158. B. Saravanakumar, S. Ramachandran, G. Ravi, V. Ganesh, R.K. Guduru, R. Yuvakkumar, Electrochemical performances of monodispersed spherical CuFe₂O₄ nanoparticles for pseudocapacitive applications. *Vacuum* **168**, 108798 (2019). <https://doi.org/10.1016/j.vacuum.2019.108798>
 159. H. Kennaz, A. Harat, O. Guellati, D.Y. Momodu, F. Barzegar, J.K. Dangbegnon, N. Manyala, M. Guerioune, Synthesis and electrochemical investigation of spinel cobalt ferrite magnetic nanoparticles for supercapacitor application. *J. Solid State Electrochem.* **22**(3), 835–847 (2017). <https://doi.org/10.1007/s10008-017-3813-y>
 160. G. Nabi, W. Raza, M.A. Kamran, T. Alharbi, M. Rafique, M.B. Tahir, S. Hussain, N. Khalid, N. Malik, R.S. Ahmed, Role of cerium-doping in CoFe₂O₄ electrodes for high performance supercapacitors. *J. Energy Storage* **29**, 101452 (2020). <https://doi.org/10.1016/j.est.2020.101452>
 161. M. Sethi, U.S. Shenoy, S. Muthu, D.K. Bhat, Facile solvothermal synthesis of NiFe₂O₄ nanoparticles for high-performance supercapacitor applications. *Front. Mater. Sci.* **14**(2), 120–132 (2020). <https://doi.org/10.1007/s11706-020-0499-3>
 162. M. Khairy, W. Bayoumy, S. Selima, M. Mousa, Studies on characterization, magnetic and electrochemical properties of nano-size pure and mixed ternary transition metal ferrites prepared by the auto-combustion method. *J. Mater. Res.* **35**(20), 2652–2663 (2020). <https://doi.org/10.1557/jmr.2020.200>
 163. B. Nawaz, G. Ali, M.O. Ullah, S. Rehman, F. Abbas, Investigation of the electrochemical properties of Ni_{0.5}Zn_{0.5}Fe₂O₄ as binder-based and binder-free electrodes of supercapacitors. *Energies* **14**(11), 3297 (2021). <https://doi.org/10.3390/en14113297>